Pertanika J. Sci. & Technol. 28 (2): 579 - 607 (2020)

PERTANIKA JOURNALS

SCIENCE & TECHNOLOGY

Journal homepage: http://www.pertanika.upm.edu.my/

Scale-3 Haar Wavelets and Quasilinearization based Hybrid Technique for the Solution of Coupled Space-Time Fractional - Burgers' Equation

Geeta Arora[1], Ratesh Kumar[1]* and Harpreet Kaur[2]

[1]Department of Mathematics, Lovely Professional University, Punjab, India
[2]Department of Mathematics, I.K. Gujral Punjab Technical University, Punjab, India

ABSTRACT

The aim of this study is to develop a hybrid method using scale 3 Haar wavelets for obtaining the solution of coupled space-time fractional Burgers' equation. Scale 3 Haar wavelets were used to estimate the solution by series approximation. Caputo and Riemann-Liouville definitions were used to handle the fractional derivatives and integrals in the problem. A quasi-linearization technique was implemented to handle the nonlinearity in the problems. Two examples of coupled space-time fractional Burgers' equations were studied to analyze the performance of the proposed technique.

Keywords: Caputo derivatives, fractional coupled Burgers' Equation, Quasi-linearization, Riemann-Liouville integration, scale 3 Haar wavelets

INTRODUCTION

Fractional calculus emerges as a great tool in explaining the physical and chemical phenomenon with alienate kinetics having microscopic complex behavior. There are fractional differential models which have a non-differentiable but continuous solution such as Weierstrass type functions (Zahle & Ziezold, 1996). These kinds of characteristics are not possible to explain with the help of ordinary or partial differential models. Earlier the field of fractional calculus was purely mathematical without any visible application but in these days, fractional calculus has gained a huge importance in the field of science and technology because of its application in the various field like theory of thermo-elasticity (Povstenko, 2009), viscoelastic fluids (Tripathi et al., 2010), dynamics of earthquakes (Lopes et al., 2013) and fluid dynamics (Momani & Odibat, 2006a). It

ARTICLE INFO

Article history:
Received: 15 September 2019
Accepted: 02 January 2020
Published: 15 April 2020

E-mail addresses:
geetadma@gmail.com (Geeta Arora)
rateshqadian@gmail.com (Ratesh Kumar)
maanh52@gmail.com (Harpreet Kaur)
* Corresponding author

ISSN: 0128-7680
e-ISSN: 2231-8526

has also been observed experimentally and from the real-time observation that there are many complex systems in the real world like relaxation in viscoelastic material, pollution diffusion in the surrounding, charge transport in amorphous semiconductors and many more which show anomalous dynamics. This capability of fractional differential equations of explaining the abnormal dynamic of the system with more efficiency and accuracy has gained huge attention from the scientific community. Many of the important classical differential equations with integer-order has got extensions to the generalized fraction differential equation with an arbitrary order for in-depth study of the corresponding physical model. But general analytic solution for many fractional differential equations which are non-homogeneous in nature are very difficult and cumbersome to achieve. Moreover, finding the solution of such equations becomes more challenging when there are nonlinearities in the equations.

Therefore, many researchers are involved in developing the various numerical and semi-analytic schemes for finding solutions to the different problems governed by these differential equations. Some of the fractional differential equations which had been recently studied because of their capability of explaining the real time phenomena's were fractional Black-Scholes equation (Duan et al., 2017), time-fractional Klein–Gordon equations (Hosseini et al., 2018; Inc et al., 2018), time-fractional Fisher's equation (Atangana, 2016; Zhang et al., 2014), fractional Bagley Torvik equation (Ray, 2012), time-fractional Burgers' equation (Inc, 2008; Khan et al., 2012), Fitzhugh–Nagumo fractional differential equation (Kumar et al., 2018), fractional Ginzburg-Landau equation (Mohebbi, 2018; Shen et al., 2018), fractional Korteweg-de Vries–Burgers' equation (Odibat & Momani, 2009; Wang, 2006), nonlinear fractional order oscillatory Van der Pol system (Ray & Patra, 2013), fractional Poisson equation (Heydari et al., 2013), fractional Riccati differential equations (Momani & Shawagfeh, 2006), fractional Schrodinger equation (Bezerra et al., 2018), fractional Sine-Gordon equations (Karayer et al., 2018), fractional Bioheat equations (Singh et al., 2011), time fractional Caudrey-Dodd-Gibbon-Sawada-Kotera equation (Baleanu et al., 2018), Sharma–Tasso–Olver equation (Roy et al., 2018), Fokker–Planck fractional equation (Mahdy & Marai, 2018; Zhang et al., 2018), fractional Telegraph equation (Momani, 2005; Tawfik et al., 2018), time-fractional generalized Boussinesq equation (Lu et al., 2018), Navier–Stokes time-fractional differential equation (Momani & Odibat, 2006b), time-fractional wave equation (Odibat & Momani, 2006) and two-dimensional fractional Helmholtz equations (Abuasad et al., 2019).

Fractional coupled Burgers' equation is also a very important equation in the field of fluid mechanics to study the motion of fluids concentrations under the effect of gravity. It is a mathematical model of time-dependent sedimentation or creaming of different concentrations of two kinds of particles in fluid colloids or suspensions, under the effect of gravity (Esipov, 1995). Burgers' equations are the special case of Navier Stokes'

equations and are very much important in the field of science and technology. Researchers are in continuous progress to study the different characteristics of the phenomenon governed by the fractional models by developing the different algorithms to solve time-fractional coupled Burgers' equation such as Fractional Variational iteration method (FVIM) (Prakash et al., 2015), Differential Transformation Method (DTM) (Liu & Hou, 2011), Homotopy Perturbation Method (HPM) (Yildirim & Kelleci, 2010), Coupled Fractional Reduced Differential Transform Method(CFRDTM) (Ray, 2013) and Adomian Decomposition Method (ADM) (Chen & An, 2008). But the study of characteristics of different concentrations of two kinds of particles governed by fractional coupled Burgers' equation has not been investigated yet by any of the scale 3 Haar wavelet-based technique simultaneously with space and time fraction.

Wavelets are one of the modernistic orthonormal functions which have the capability of dilation and translation. Because of these properties, numerical techniques that involve wavelet bases are showing the qualitative improvement in contrast with other methods. In literature, dyadic wavelets are in preponderance. In 1995, Chui and Lian had developed the scale 3 Haar wavelets by using the process of multiresolution analysis. In 2018, Mittal and Pandit (2018a, 2018b & 2019) had used the scale 3 Haar wavelets for solving the various types of differential equations and found that these wavelet bases were equally competent in solving the various types of mathematical models governed by differential equations. Also, it was shown by them that the scale 3 Haar wavelet had a faster rate of convergence as compared to the dyadic wavelets. Moreover, investigation of characteristics of the solution to the fractional coupled Burgers' equation has not been done yet by the Scale 3 Haar wavelet methods as far as our knowledge is concerned. This encourages us to develop a new technique using scale 3 Haar wavelet for analyzing the behavior of systems governed by the fractional coupled Burgers' equation.

The prime objective of the proposed work is to provide a new numerical technique for obtaining the solution of space-time fractional-coupled Burgers' equation (Equation 1) emerging in the field of fluid dynamics using scale 3 Haar wavelet bases

$$\begin{cases} \dfrac{\partial^{\alpha} u}{\partial t^{\alpha}} = \dfrac{\partial^2 u}{\partial x^2} - \eta\, u \dfrac{\partial^{\beta} u}{\partial x^{\beta}} - \mu \dfrac{\partial (uv)}{\partial x} \quad , \qquad x \in [\mathrm{a}\,, \mathrm{b}] \quad , t \in [0, T \\ \dfrac{\partial^{\gamma} v}{\partial t^{\gamma}} = \dfrac{\partial^2 v}{\partial x^2} - \xi\, v \dfrac{\partial^{\delta} v}{\partial x^{\delta}} - \lambda \dfrac{\partial (uv)}{\partial x} \quad , \qquad x \in [\mathrm{a}\,, \mathrm{b}] \quad , t \in [0, T \end{cases} \tag{1}$$

subjected to the boundary constraints (Equation 2)

$$u(a,t) = f_1(t)\ , u(b,t) = f_2(t)\ , \qquad v(a,t) = \varphi_1(t)\ , v(b,t) = \varphi_2(t) \quad \forall t \in [0,T] \tag{2}$$

and with the constraints at the initial value (Equation 3)

$$u(x,0) = h(x) \quad , \quad v(x,0) = p(x) \qquad \forall \ \ x \in [a\ ,b] \tag{3}$$

where $\alpha, \beta, \gamma, \delta$ represents the order of fractional derivatives such that $0 < \alpha, \beta, \gamma, \delta \leq 1$. Different variations can be observed in the solution space by giving different values to these four parameters $\alpha, \beta, \gamma, \delta$. However, on taking $\alpha = \beta = \gamma = \delta = 1$ the fractional-coupled Burgers' equation will respond like a classical coupled Burgers' equation with integer order. η, ξ, μ, λ are arbitrary constants depending upon the system parameter like Peclet number and Reynold number.

The manuscript follows the sequence of sections as described: In section 2, explicit forms of scale 3 Haar wavelets with their families and procedure to find their integrals have been explained briefly. Representation of the solution using scale 3 Haar wavelets is explained in section 3. Section 4 explains the method of solution using scale 3 Haar wavelets. In section 5, the convergence of the method is discussed. In section 6, solutions of two different coupled Burgers' fractional equations are produced using the present method to analyze the efficiency and performance of the present method. In section 7, the conclusion drawn from the results and future research ideas are given.

Scale 3 Haar Wavelets and its Integrals

The mathematical expressions for father wavelet (Scale 3 Haar function) and mother wavelets for scale 3 Haar wavelet family with dilation factor three (Chui & Lian, 1995; Mittal & Pandit, 2018a) are given in Equation 4, 5 and 6

$$\text{Haar scaling function } h_1(t) = \begin{cases} 1 & 0 \leq t < 1 \\ 0 & elsewhere \end{cases} \tag{4}$$

$$h_i(t) = \psi^1\left(3^j t - k\right) = \frac{1}{\sqrt{2}} \begin{cases} -1 & \alpha_1(i) \leq t < \alpha_2(i) \\ 2 & \alpha_2(i) \leq t < \alpha_3(i) \\ -1 & \alpha_3(i) \leq t < \alpha_4(i) \\ 0 & elsewhere \end{cases}, \ for \ i = 2,4, \ldots 3p-1 \tag{5}$$

$$h_i(t) = \psi^2\left(3^j t - k\right) = \sqrt{\frac{3}{2}} \begin{cases} 1 & \alpha_1(i) \leq t < \alpha_2(i) \\ 0 & \alpha_2(i) \leq t < \alpha_3(i) \\ -1 & \alpha_3(i) \leq t < \alpha_4(i) \\ 0 & elsewhere \end{cases}, \qquad for \quad i = 3,6, \ldots 3p \tag{6}$$

where $\alpha_1(i) = \frac{k}{p}, \alpha_2(i) = \frac{3k+1}{3p}, \alpha_3(i) = \frac{(3k+2)}{3p}, \alpha_4(i) = \frac{k+1}{p}, p = 3^j \ , j = 0,1,2, \ldots ,$ $k = 0,1,2, \ldots, p-1.$

Here *i, j, k* respectively represent the wavelet number, level of resolution (dilation) and translation parameters of wavelet family. The values of *i* (*for i* > 1) can be calculated with the help of *j, k* by using the following relations $i - 1 = 3^j + 2k$ for even values of *i* and $i - 2 = 3^j + 2k$ for odd values of *i*. By using this relation for different dilation and translations of $h_2(t)$, $h_3(t)$ we will get the wavelet family as $h_1(t)$, $h_2(t)$, $h_3(t)$, $h_4(t)$, $h_5(t)$, $h_6(t)$... where $h_2(t)$ and $h_3(t)$ are also called mother wavelets and rest all the wavelets which we have obtained from mother wavelets are called daughter wavelets.

The main difference which makes the scale 3 Haar wavelets better than the dyadic wavelets is that only one mother wavelet is responsible for the construction of whole wavelet family but in case of scale 3 Haar wavelets, two mother wavelets with different shapes are responsible for the construction of the whole family. Because of this fact, scale 3 Haar wavelets increase the convergence rate of the solution. The construction of scale 3 Haar wavelet family is done by using the properties of Multi-resolution analysis which are described below

Now one can easily integrate the equations (Equation 4, 5 and 6) with the desired number of times over the interval [A, B) by using Riemann Liouville Integral formula (Das, 2011) as given in Equation 7

$$q_{\beta,i}(t) = \frac{1}{\Gamma(\beta)}\int_A^t h_i(x)(t-x)^{\beta-1}dx$$

$$\forall \quad 0 \le \beta \le m\,, \qquad m = 1,2,3 \ldots\ldots\,, \qquad i = 1,2,3, \ldots\ldots 3p \tag{7}$$

After evaluating the above integrals for Equation 4, we get Equation 8

$$q_{\beta,i}(t) = \frac{t^{\beta}}{\Gamma(\beta+1)} \quad \text{for } i = 1 \tag{8}$$

Using Equation 7 on Equation 5, we get the values of $q_{\beta,i}(t)$*'s for* $i = 2,4,6,8\ldots,3p-1$ are given by Equation 9

$$q_{\beta,i}(t) = \frac{1}{\sqrt{2}}\begin{cases} 0 & for \quad 0 \le t \le \alpha_1(i) \\ \frac{-1}{\Gamma(\beta+1)}\left(t-\alpha_1(i)\right)^{\beta} & for \quad \alpha_1(i) \le t \le \alpha_2(i) \\ \frac{1}{\Gamma(\beta+1)}\left[-\left(t-\alpha_1(i)\right)^{\beta}+3\left(t-\alpha_2(i)\right)^{\beta}\right] & for \quad \alpha_2(i) \le t \le \alpha_3(i) \\ \frac{1}{\Gamma(\beta+1)}\left[-\left(t-\alpha_1(i)\right)^{\beta}+3\left(t-\alpha_2(i)\right)^{\beta}-3\left(t-\alpha_3(i)\right)^{\beta}\right] & for\ \alpha_3(i) \le t \le \alpha_4(i) \\ \frac{1}{\Gamma(\beta+1)}\left[-\left(t-\alpha_1(i)\right)^{\beta}+3\left(t-\alpha_2(i)\right)^{\beta}-3\left(t-\alpha_3(i)\right)^{\beta}+\left(t-\alpha_4(i)\right)^{\beta}\right] & for\ \alpha_4(i) \le t \le 1 \end{cases} \tag{9}$$

Using Equation 7 on Equation 6, we get the values of $q_{\beta,i}(t)$*'s for* $i = 3,5,7,9\ldots,3p$ which are given by Equation 10

$$q_{\beta,i}(t) = \sqrt{\frac{3}{2}} \begin{cases} 0 & for \quad 0 \le t \le \alpha_1(i) \\ \frac{1}{\Gamma(\beta+1)}(t-\alpha_1(i))^{\beta} & for \quad \alpha_1(i) \le t \le \alpha_2(i) \\ \frac{1}{\Gamma(\beta+1)}[(t-\alpha_1(i))^{\beta} - (t-\alpha_2(i))^{\beta}] & for \quad \alpha_2(i) \le t \le \alpha_3(i) \\ \frac{1}{\Gamma(\beta+1)}[(t-\alpha_1(i))^{\beta} - (t-\alpha_2(i))^{\beta} - (t-\alpha_3(i))^{\beta}] & for \quad \alpha_3(i) \le t \le \alpha_4(i) \\ \frac{1}{\Gamma(\beta+1)}[(t-\alpha_1(i))^{\beta} - (t-\alpha_2(i))^{\beta} - (t-\alpha_3(i))^{\beta} + (t-\alpha_4(i))^{\beta}] & for \ \alpha_4(i) \le t \le 1 \end{cases} \tag{10}$$

Approximation of Solution

Using the properties of scale 3 Haar wavelets, any function $x(t) \in L_2(R)$ can be expressed as given in Equation 11

$$u(t) = \sum_{i=0}^{\infty} a_i h_i(t) = a_1 h_1(t) + \sum_{even\, i} a_i \psi^1(3^j t - k) + \sum_{odd\, i} a_i \psi^2(3^j t - k) \tag{11}$$

Here a_i'*s* are the wavelet coefficients whose values are to be determined by the proposed method. But for computational purpose, one can consider a finite number of terms. By considering the first 3*p* terms to approximate the function *u*(*t*) we get Equation 12

$$u(t) \approx u_{3p} = \sum_{i=0}^{3p} a_i h_i(t) \tag{12}$$

where $p = 3^j$, $j = 0, 1, 2 \ldots$

METHOD OF SOLUTION

By applying the quasi-linearization technique to linearize the non-linear terms of Equation 1, 2 and 3, we get the equivalent expression given by Equaion 13, 14, 15 and 16

$$(uv_x)_{r+1} = u_{r+1}(v_x)_r + u_r(v_x)_{r+1} - u_r(v_x)_r \tag{13}$$

$$(vu_x)_{r+1} = v_{r+1}(u_x)_r + v_r(u_x)_{r+1} - v_r(u_x)_r \tag{14}$$

$$(uu_\beta)_{r+1} = u_{r+1}(u_\beta)_r + u_r(u_\beta)_{r+1} - u_r(u_\beta)_r \tag{15}$$

$$(vv_\delta)_{r+1} = v_{r+1}(v_\delta)_r + v_r(v_\delta)_{r+1} - v_r(v_\delta)_r \tag{16}$$

Using Equation 13, 14, 15 and 16, non-linear coupled fractional differential Equation 1, 2 and 3 transformed into a sequence of linear differential Equations 17 and 18

$$\left(\frac{\partial^{\alpha}u}{\partial t^{\alpha}}\right)_{r+1} = (u_{xx})_{r+1} - \eta\left(u_{r+1}(u_{\beta})_{r} + u_{r}(u_{\beta})_{r+1} - u_{r}(u_{\beta})_{r}\right) - \mu[(u_{r+1}(v_{x})_{r} + u_{r}(v_{x})_{r+1} - u_{r}(v_{x})_{r}) + (v_{r+1}(u_{x})_{r} + v_{r}(u_{x})_{r+1} - v_{r}(u_{x})_{r})] \quad (17)$$

$$\left(\frac{\partial^{\gamma}v}{\partial t^{\gamma}}\right)_{r+1} = (u_{xx})_{r+1} - \xi(v_{r+1}(v_{\delta})_{r} + v_{r}(v_{\delta})_{r+1} - v_{r}(v_{\delta})_{r}) - \lambda[(u_{r+1}(v_{x})_{r} + u_{r}(v_{x})_{r+1} - u_{r}(v_{x})_{r}) + (v_{r+1}(u_{x})_{r} + v_{r}(u_{x})_{r+1} - v_{r}(u_{x})_{r})] \quad (18)$$

subjected to the boundary constraints given by Equation 19

$$u(a,t_{r+1}) = f_{1}(t_{r+1}) \quad , u(b,t_{r+1}) = f_{2}(t_{r+1}) \ , \ v(a,t_{r+1}) = \varphi_{1}(t_{r+1}) \qquad v(b,t_{r+1}) = \varphi_{2}(t_{r+1}) \quad (19)$$

and with the constraints on initial values given by Equation 20

$$u(x,0) = h(x), v(x,0) = p(x), \forall \ \mathrm{x} \in [\mathrm{a}\,,\mathrm{b}] \ , t_{r+1} \in [0,T] \text{ and } r = 0,1,2\cdots m-1 \quad (20)$$

here t_{r+1} represents $(r+1)^{\text{th}}$ approximation for t in the process of quasilinearization.

$$\dot{u_{xx}}(x,t) = \sum_{i=1}^{3m} a_{i}h_{i}(x) \quad (21)$$

$$\dot{v_{xx}}(x,t) = \sum_{i=1}^{3m} b_{i}h_{i}(x) \quad (22)$$

Integrating the Equation 21 and 22 with respect to t from t_{r} to t_{r+1} to we get

$$u_{xx}(x,t_{r+1}) = (t_{r+1} - t_{r}) \sum_{i=1}^{3m} a_{i}h_{i}(x) + u_{xx}(x,t_{r}) \quad (23)$$

$$v_{xx}(x,t_{r+1}) = (t_{r+1} - t_{r}) \sum_{i=1}^{3m} b_{i}h_{i}(x) + v_{xx}(x,t_{r}) \quad (24)$$

Now integrating Equation 23 and 24 with respect to x within the limits 0 to x we get

$$u_{x}(x,t_{r+1}) = (t_{r+1} - t_{r}) \sum_{i=1}^{3m} a_{i}q_{i,1}(x) + u_{x}(x,t_{r}) + \left(u_{x}(0,t_{r+1}) - u_{x}(0,t_{r})\right) \quad (25)$$

$$v_x(x,t_{r+1}) = (t_{r+1} - t_r)\sum_{i=1}^{3m} b_i q_{i,1}(x) + v_x(x,t_r) + \left(v_x(0,t_{r+1}) - v_x(0,t_r)\right) \quad (26)$$

Again, integrating the Equation 25 and 26 with respect to x within the limits 0 to x we get

$$u(x,t_{r+1}) = (t_{r+1} - t_r)\sum_{i=1}^{3m} a_i q_{i,2}(x) + \left(u(x,t_r) - u(0,t_r)\right) + x\left(u_x(0,t_{r+1}) - u_x(0,t_r)\right) + u(0,t_{r+1}) \quad (27)$$

$$v(x,t_{r+1}) = (t_{r+1} - t_r)\sum_{i=1}^{3m} b_i q_{i,2}(x) + \left(v(x,t_r) - v(0,t_r)\right) + x\left(v_x(0,t_{r+1}) - v_x(0,t_r)\right) + v(0,t_{r+1}) \quad (28)$$

on substitute the values of unknown quantities $u_x(0,t_{r+1}) - u_x(0,t_r)$, $v_x(0,t_{r+1}) - v_x(0,t_r)$ by evaluating it from the above equations using $x = 1$ in the Equation 27 and 28, we get

$$u(x,t_{r+1}) = (t_{r+1} - t_r)\sum_{i=1}^{3m} a_i(q_{i,2}(x) - x\,q_{i,2}(1)) + \left(u(x,t_r) - u(0,t_r)\right) + x\left(u(1,t_{r+1}) - u(0,t_{r+1})\right) - x\left(u(1,t_r) - u(0,t_r)\right) + u(0,t_{r+1}) \quad (29)$$

$$v(x,t_{r+1}) = (t_{r+1} - t_r)\sum_{i=1}^{3m} b_i(q_{i,2}(x) - x\,q_{i,2}(1)) + \left(v(x,t_r) - v(0,t_r)\right) + x\left(v(1,t_{r+1}) - v(0,t_{r+1})\right) - x\left(v(1,t_r) - v(0,t_r)\right) + v(0,t_{r+1}) \quad (30)$$

$$u_x(x,t_{r+1}) = (t_{r+1} - t_r)\sum_{i=1}^{3m} a_i\left(q_{i,1}(x) - q_{i,2}(1)\right) + u_x(x,t_r) + \left(u(1,t_{r+1}) - u(0,t_{r+1})\right) - \left(u(1,t_r) - u(0,t_r)\right) \quad (31)$$

$$v_x(x,t_{r+1}) = (t_{r+1} - t_r)\sum_{i=1}^{3m} b_i(q_{i,1}(x) - q_{i,2}(1)) + v_x(x,t_r) + \left(v(1,t_{r+1}) - v(0,t_{r+1})\right) - \left(v(1,t_r) - v(0,t_r)\right) \quad (32)$$

$$\frac{\partial^\alpha u}{\partial t^\alpha}(x,t_{r+1}) = \frac{(t_{r+1} - t_r)^{1-\alpha}}{\Gamma(2-\alpha)}\sum_{i=1}^{3m} a_i(q_{i,2}(x) - x\,q_{i,2}(1)) + x\,\frac{\partial^\alpha}{\partial t^\alpha}\left(u(1,t_{r+1}) - u(0,t_{r+1})\right) + \frac{\partial^\alpha u}{\partial t^\alpha}(0,t_{r+1}) \quad (33)$$

$$\frac{\partial^{\beta} u}{\partial x^{\beta}}(x,t_{r+1}) = (t_{r+1} - t_r)\sum_{i=1}^{3m} a_i\left(q_{i,2-\beta}(x) - \frac{x^{\beta}}{\Gamma(2-\beta)} q_{i,2}(1)\right) + \frac{\partial^{\beta} u}{\partial x^{\beta}}(x,t_r) + \frac{x^{\beta}}{\Gamma(2-\beta)}\left[\left(u(1,t_{r+1}) - u(0,t_{r+1})\right) - \left(u(1,t_r) - u(0,t_r)\right)\right] \quad (34)$$

$$\frac{\partial^{\gamma} v}{\partial t^{\gamma}}(x,t_{r+1}) = \frac{(t_{r+1} - t_r)^{1-\gamma}}{\Gamma(2-\gamma)} \sum_{i=1}^{3m} b_i\left(q_{i,2}(x) - x\, q_{i,2}(1)\right) + x\, \frac{\partial^{\alpha}}{\partial t^{\alpha}}\left(v(1,t_{r+1}) - v(0,t_{r+1})\right) + \frac{\partial^{\alpha} v}{\partial t^{\alpha}}(0,t_{r+1}) \quad (35)$$

$$\frac{\partial^{\delta} v}{\partial x^{\delta}}(x,t_{r+1}) = (t_{r+1} - t_r)\sum_{i=1}^{3m} a_i\left(q_{i,2-\delta}(x) - \frac{x^{\delta}}{\Gamma(2-\delta)} q_{i,2}(1)\right) + \frac{\partial^{\delta} v}{\partial x^{\delta}}(x,t_r) + \frac{x^{\delta}}{\Gamma(2-\delta)}\left[\left(v(1,t_{r+1}) - v(0,t_{r+1})\right) - \left(v(1,t_r) - v(0,t_r)\right)\right] \quad (36)$$

Now using the boundary constraints and discretizing the space variable as $x \to x_l$ where $x_l = \frac{2l-1}{6p}$, $l = 0,1,2,\ldots\ldots 2p$ in the Equation 29, 30, 31, 32, 33, 34, 35 and 36 and substituting the values obtained in Equation 17 and 18 the following system of equations (Equation 37) are obtained for different values of *r*

$$\left.\begin{aligned} a_{1\times 3p} A_{3p\times 3p} + b_{1\times 3p} B_{3p\times 3p} &= C_{1\times 3p} \\ b_{1\times 3p}\, D_{3p\times 3p} + a_{1\times 3p} E_{3p\times 3p} &= F_{1\times 3p} \end{aligned}\right\} \quad (37)$$

Where the Equation 38,39,40,41,42 and 43 respectivelyb represents the values of *A, B, C, D, E* and *F* as

$$A = \begin{bmatrix} \frac{(t_{r+1} - t_r)^{1-\alpha}}{\Gamma(2-\alpha)}\left(q_{i,2}(x_l) - x_l\, q_{i,2}(1)\right) \\ -(t_{r+1} - t_r)\left\{ \begin{array}{c} h_i(x_l) - \eta\left(\begin{array}{c} \left(u_{\beta}\right)_r\left(q_{i,2}(x_l) - x_l\, q_{i,2}(1)\right) \\ +u_r\left(q_{i,2-\beta}(x_l) - \frac{{x_l}^{\beta}}{\Gamma(2-\beta)}\left(q_{i,2}(1)\right)\right) \end{array}\right) \\ -\mu\left(\left(v_x\right)_r\left(q_{i,2}(x_l) - x_l\, q_{i,2}(1)\right) + v_r\left(q_{i,1}(x_l) - q_{i,2}(1)\right)\right) \end{array}\right\} \end{bmatrix} \quad (38)$$

$$B = \left[\mu\,(t_{r+1} - t_r)\left(\left(u_x\right)_r\left(q_{i,2}(x_l) - x_l\, q_{i,2}(1)\right) + u_r\left(q_{i,1}(x_l) - q_{i,2}(1)\right)\right)\right] \quad (39)$$

$$
\begin{aligned}
C = \; & u_{xx}(x_l, t_r) \\
& - \eta \Bigg[(u_\beta)_r \Big(\big(u(x_l, t_r) - f_1(t_r)\big) + x_l \big(f_2(t_{r+1}) - f_1(t_{r+1})\big) - x_l \big(f_2(t_r) - f_1(t_r)\big) + f_1(t_{r+1}) \Big) \\
& + u_r \left(\frac{\partial^\beta u}{\partial x^\beta}(x_l, t_r) + \frac{{x_l}^\beta}{\Gamma(2-\beta)} \Big(\big(f_2(t_{r+1}) - f_1(t_{r+1})\big) - \big(f_2(t_r) - f_1(t_r)\big) \Big) \right) - u_r (u_\beta)_r \Bigg] \\
& - \mu \Big[\Big\{ (v_x)_r \Big(\big(u(x_l, t_r) - f_1(t_r)\big) + x_l \big(f_2(t_{r+1}) - f_1(t_{r+1})\big) - x_l \big(f_2(t_r) - f_1(t_r)\big) + f_1(t_{r+1}) \Big) \\
& + u_r \Big(v_x(x_l, t_r) + \big((\varphi_2(t_{r+1}) - \varphi_1(t_{r+1})) \big) - \big((\varphi_2(t_r) - \varphi_1(t_r)) \big) \Big) - u_r (v_x)_r \Big\} \\
& + (u_x)_r \Big(\big(v(x_l, t_r) - \varphi_1(t_r)\big) + x_l \big((\varphi_2(t_{r+1}) - \varphi_1(t_{r+1})) \big) - x_l \big((\varphi_2(t_r) - \varphi_1(t_r)) \big) + \varphi_1(t_{r+1}) \Big) \\
& + v_r \Big(u_x(x_l, t_r) + \big(f_2(t_{r+1}) - f_1(t_{r+1})\big) - \big((\varphi_2(t_r) - \varphi_1(t_r)) \big) \Big) - v_r (u_x)_r \Big] \\
& - x_l \left(\frac{\partial^\alpha}{\partial t^\alpha} \big(f_2(t) - f_1(t)\big) \right)_{t = t_{r+1}} - \left(\frac{\partial^\alpha f_1(t)}{\partial t^\alpha} \right)_{t = t_{r+1}}
\end{aligned} \tag{40}
$$

$$
\begin{aligned}
D = \; & \Bigg[\frac{(t_{r+1} - t_r)^{1-\gamma}}{\Gamma(2-\gamma)} \Big(q_{i,2}(x_l) - x_l \, q_{i,2}(1) \Big) \\
& - (t_{r+1} - t_r) \Bigg\{ h_i(x_l) - \xi \left((v_\delta)_r \Big(q_{i,2}(x_l) - x_l \, q_{i,2}(1) \Big) + v_r \left(q_{i,2-\delta}(x_l) - \frac{{x_l}^\delta}{\Gamma(2-\delta)} \Big(q_{i,2}(1) \Big) \right) \right) \\
& - \lambda \Big((u_x)_r \Big(q_{i,2}(x_l) - x_l \, q_{i,2}(1) \Big) + u_r \Big(q_{i,1}(x_l) - q_{i,2}(1) \Big) \Big) \Bigg\} \Bigg]
\end{aligned} \tag{41}
$$

$$
E = \Big[\lambda (t_{r+1} - t_r) \Big((v_x)_r \Big(q_{i,2}(x_l) - x_l \, q_{i,2}(1) \Big) + v_r \Big(q_{i,1}(x_l) - q_{i,2}(1) \Big) \Big) \Big] \tag{42}
$$

$$
\begin{aligned}
F = \; & v_{xx}(x_l, t_r) \\
& - \xi \Big[(v_\delta)_r \Big(\big(v(x_l, t_r) - \varphi_1(t_r)\big) + x_l \big(\varphi_2(t_{r+1}) - \varphi_1(t_{r+1})\big) - x_l \big(\varphi_2(t_r) - \varphi_1(t_r)\big) + \varphi_1(t_{r+1}) \Big) \\
& + v_r \left(\frac{\partial^\delta v}{\partial x^\delta}(x_l, t_r) + \frac{{x_l}^\delta}{\Gamma(2-\delta)} \Big(\big(\varphi_2(t_{r+1}) - \varphi_1(t_{r+1})\big) - \big(\varphi_2(t_r) - \varphi_1(t_r)\big) \Big) \right) - v_r (v_\delta)_r \Big] \\
& - \lambda \Big[\Big\{ (v_x)_r \Big(\big(u(x_l, t_r) - f_1(t_r)\big) + x_l \big(f_2(t_{r+1}) - f_1(t_{r+1})\big) - x_l \big(f_2(t_r) - f_1(t_r)\big) + f_1(t_{r+1}) \Big) \\
& + u_r \big(v_x(x_l, t_r) + \big(\varphi_2(t_{r+1}) - \varphi_1(t_{r+1})\big) - \big(\varphi_2(t_r) - \varphi_1(t_r)\big) \big) - u_r (v_x)_r \Big\} \\
& + (u_x)_r \Big(\big(v(x_l, t_r) - \varphi_1(t_r)\big) + x_l \big(\varphi_2(t_{r+1}) - \varphi_1(t_{r+1})\big) - x_l \big(\varphi_2(t_r) - \varphi_1(t_r)\big) + \varphi_1(t_{r+1}) \Big) \\
& + v_r \Big(u_x(x_l, t_r) + \big(f_2(t_{r+1}) - f_1(t_{r+1})\big) - \big(f_2(t_r) - f_1(t_r)\big) \Big) - v_r (u_x)_r \Big] \\
& - x_l \left(\frac{\partial^\alpha}{\partial t^\alpha} \big(\varphi_2(t) - \varphi_1(t)\big) \right)_{t = t_{r+1}} - \left(\frac{\partial^\alpha \varphi_1(t)}{\partial t^\alpha} \right)_{t = t_{r+1}}
\end{aligned} \tag{43}
$$

The process of the solution starts by taking $r = 0$, $t_0 = 0$ and the boundary conditions given in Equation 44 as

$$u(x_l,t_r) = u(x_l,0) = h(x_l), u_x(x_l,t_r) = u_x(x_l,0) = h_x(x_l),$$
$$u_{xx}(x_l,t_r) = u_{xx}(x_l,0) = h_{xx}(x_l)$$

$$v(x_l,t_r) = v(x_l,0) = p(x_l), v_x(x_l,t_r) = v_x(x_l,0) = p_x(x_l),$$
$$v_{xx}(x_l,t_r) = v_{xx}(x_l,0) = p_{xx}(x_l) \quad (44)$$

The values of wavelet coefficients can be calculated successively for different values of $r = 0, 1, 2 \ldots$ by using the Equation 45 and 46

$$a_{1\times 3p} = (C - FD^{-1}B) * (A - ED^{-1}B) \quad (45)$$

$$b_{1\times 3p} = (C - FE^{-1}A) * (B - DE^{-1}A) \quad (46)$$

Then by putting the values of the wavelet coefficient a_i's and b_i's in the Equation 49 and 50 one can obtain numerically approximated solution successively for $u(x,t)$ and $v(x,t)$ for $r = 0, 1, 2, 3 \ldots$ using Equation 47 and 48

$$u(x_l,t_{r+1}) = (t_{r+1} - t_r) \sum_{i=1}^{3m} a_i (q_{i,2}(x_l) - x_l q_{i,2}(1)) + \left(u(x_l,t_r) - f_1(t_r)\right) + x_l\left(f_2(t_{r+1}) - f_1(t_{r+1})\right) - x_l\left(f_2(t_r) - f_1(t_r)\right) + f_1(t_{r+1}) \quad (47)$$

$$v(x_l,t_{r+1}) = (t_{r+1} - t_r) \sum_{i=1}^{3m} b_i (q_{i,2}(x_l) - x_l q_{i,2}(1)) + \left(v(x_l,t_r) - \varphi_1(t_r)\right) + x_l\left(\varphi_2(t_{r+1}) - \varphi_1(t_{r+1})\right) - x_l\left(\varphi_2(t_r) - \varphi_1(t_r)\right) + \varphi_1(t_{r+1}) \quad (48)$$

at various times by using successive iteration for $r = 0, 1, 2, 3 \ldots$

Convergence Analysis

To establish the convergence of the proposed method, we considered the asymptotic extension of Equation 47 and 48 for a fixed value of $t = t_{r+1}$ and $x = x_1$ as given below (Equation 49 and 50)

$$u(x,t) = \Delta t * \sum_{i=1}^{\infty} a_i (q_{i,2}(x) - x\, q_{i,2}(1)) + A + Bx,$$
Where $A = u(x_l,t_r) + f_1(t_{r+1}) - f_1(t_r)$,
$$B = \left(f_2(t_{r+1}) - f_1(t_{r+1})\right) - \left(f_2(t_r) - f_1(t_r)\right) \quad (49)$$

$$v(x,t) = \Delta t * \sum_{i=1}^{\infty} b_i(q_{i,2}(x_l) - x\, q_{i,2}(1)) + C + Dx \ ,$$

Where $C = \big(v(x_l,t_r) - \varphi_1(t_r)\big) + \varphi_1(t_{r+1})$,

$$D = \big(\varphi_2(t_{r+1}) - \varphi_1(t_{r+1})\big) - \big(\varphi_2(t_r) - \varphi_1(t_r)\big) \tag{50}$$

Now the convergence of the theorem will be proven with the help of the following lemma

Lemma 1: let $u(x)\epsilon L^2(R)$ be any square-integrable function such that $|u^m(x)| \le M, \forall\ x\epsilon(0,1)$ and $D_*^{\alpha}u(x) = \sum_{i=1}^{\infty} a_i h_i(x)$. Then $|a_i| \le \frac{2\sqrt{2}\,M}{3\Gamma(m-\alpha+1)} \times \frac{1}{3^{j\left(m-\alpha+\frac{1}{2}\right)}}$

Proof: Let $D_*^{\alpha}u(x) = \sum_{i=1}^{\infty} a_i h_i(x)$ be the exact solution and $D_*^{\alpha}u_{3p}(x) = \sum_{i=1}^{3p} a_i h_i(x)$ be the approximated solution

Now the error at the J^{th} level of resolution can be represented by Equation 51 and the value of a_i is given by Equation 52

$$\left\|E_j\right\|^2 = \left\|D_*^{\alpha}u(x) - D_*^{\alpha}u_{3p}(x)\right\|^2 = \left\|\sum_{i=3p+1}^{\infty} a_i h_i(x)\right\|^2 =$$

$$\left\langle \sum_{i=3p+1}^{\infty} a_i h_i(x)\ ,\sum_{i=3p+1}^{\infty} a_i h_i(x) \right\rangle$$

$$= \int_{-\infty}^{\infty} \sum_{i=3p+1}^{\infty} \sum_{k=3p+1}^{\infty} a_i a_k h_i(x) h_k(x)\, dx = \sum_{i=3p+1}^{\infty} \sum_{k=3p+1}^{\infty} a_i a_k \int_0^1 h_i(x) h_k(x)\, dx$$

$$= \sum_{i=3p+1}^{\infty} a_i a_i = \sum_{i=3p+1}^{\infty} |a_i|^2 \tag{51}$$

$$a_i = 3^{\frac{j}{2}} \int_0^1 h_i(x)\, D_*^{\alpha}u(x)dx = 3^{\frac{j}{2}} \left(\int_0^1 {\psi_i}^1(x)\, D_*^{\alpha}u(x)dx + \int_0^1 {\psi_i}^2(x)\, D_*^{\alpha}u(x)dx \right)$$

$$= 3^{\frac{j}{2}} \left[\begin{array}{c} \left(\int_{\alpha_1(i)}^{\alpha_2(i)} \frac{-1}{\sqrt{2}} D_*^{\alpha}u(x)dx + \int_{\alpha_2(i)}^{\alpha_3(i)} \sqrt{2}\, D_*^{\alpha}u(x)dx + \int_{\alpha_3(i)}^{\alpha_4(i)} \frac{-1}{\sqrt{2}} D_*^{\alpha}u(x)dx \right) + \\ \left(\int_{\alpha_1(i)}^{\alpha_2(i)} \frac{\sqrt{3}}{2} D_*^{\alpha}u(x)dx + \int_{\alpha_3(i)}^{\alpha_4(i)} \frac{-\sqrt{3}}{2} D_*^{\alpha}u(x)dx \right) \end{array} \right] \tag{52}$$

By applying the mean value theorem (Sahoo & Riedel, 1998) of integralon on Equation 52 , we get $\varepsilon_1 \in \left(\alpha_1(i), \alpha_2(i)\right), \varepsilon_2 \in \left(\alpha_2(i), \alpha_3(i)\right), \varepsilon_3 \in \left(\alpha_3(i), \alpha_4(i)\right)$ (Equation 53) such that

$$\int_{\alpha_1(i)}^{\alpha_2(i)} D_*^{\alpha} u(x)dx = (\alpha_2(i) - \alpha_1(i)) D_*^{\alpha} u(\varepsilon_1) = \frac{1}{3p} D_*^{\alpha} u(\varepsilon_1)$$

$$\int_{\alpha_2(i)}^{\alpha_3(i)} D_*^{\alpha} u(x)dx = (\alpha_3(i) - \alpha_2(i)) D_*^{\alpha} u(\varepsilon_2) = \frac{1}{3p} D_*^{\alpha} u(\varepsilon_2)$$

$$\int_{\alpha_3(i)}^{\alpha_4(i)} D_*^{\alpha} u(x)dx = (\alpha_4(i) - \alpha_3(i)) D_*^{\alpha} u(\varepsilon_3) = \frac{1}{3p} D_*^{\alpha} u(\varepsilon_3) \tag{53}$$

Now using Equation 53 ,Equation 52 becomes Equation 54

$$a_i = \frac{3^{\frac{j}{2}}}{3p}\left(\left(\frac{\sqrt{3}-1}{\sqrt{2}}\right) D_*^{\alpha} u(\varepsilon_1) + \sqrt{2} D_*^{\alpha} u(\varepsilon_2) - \left(\frac{\sqrt{3}-1}{\sqrt{2}}\right) D_*^{\alpha} u(\varepsilon_3)\right)$$

$$= \frac{3^{\frac{j}{2}}}{3p}\left(\left(\frac{\sqrt{3}-1}{\sqrt{2}}\right) D_*^{\alpha} u(\varepsilon_1) + \sqrt{2} D_*^{\alpha} u(\varepsilon_2) - \left(\frac{\sqrt{3}-1}{\sqrt{2}}\right) D_*^{\alpha} u(\varepsilon_3)\right)$$

$$= 3^{\frac{-j-2}{2}}\left(\left(\frac{\sqrt{3}-1}{\sqrt{2}}\right) D_*^{\alpha} u(\varepsilon_1) + \sqrt{2} D_*^{\alpha} u(\varepsilon_2) - \left(\frac{\sqrt{3}-1}{\sqrt{2}}\right) D_*^{\alpha} u(\varepsilon_3)\right) \tag{54}$$

Now by using the Caputo definition of fractional derivatives (Das, 2011) on Equation 54, we get Equation 55,

$$a_i = 3^{\frac{-j-2}{2}}\left(\begin{array}{c}\left(\frac{\sqrt{3}-1}{\sqrt{2}}\right)\left(\frac{1}{\Gamma(m-\alpha)}\int_0^{\varepsilon_1} \frac{u^m(z)}{(\varepsilon_1 - z)^{\alpha-m+1}} dz\right) + \sqrt{2}\left(\frac{1}{\Gamma(m-\alpha)}\int_0^{\varepsilon_2} \frac{u^m(z)}{(\varepsilon_2 - z)^{\alpha-m+1}} dz\right) \\ - \left(\frac{\sqrt{3}-1}{\sqrt{2}}\right)\left(\frac{1}{\Gamma(m-\alpha)}\int_0^{\varepsilon_3} \frac{u^m(z)}{(\varepsilon_3 - z)^{\alpha-m+1}} dz\right)\end{array}\right)$$

$$= \frac{3^{\frac{-j-2}{2}}}{\sqrt{2}\,\Gamma(m-\alpha)}\left(\begin{array}{c}\left(\sqrt{3}-1\right)\int_0^{\varepsilon_1} \frac{u^m(z)}{(\varepsilon_1 - z)^{\alpha-m+1}} dz - 2\int_{\varepsilon_2}^{0} \frac{u^m(z)}{(\varepsilon_2 - z)^{\alpha-m+1}} dz \\ -\left(\sqrt{3}-1\right)\left(\int_0^{\varepsilon_1} \frac{u^m(z)}{(\varepsilon_3 - z)^{\alpha-m+1}} dz + \int_{\varepsilon_1}^{\varepsilon_3} \frac{u^m(z)}{(\varepsilon_3 - z)^{\alpha-m+1}} dz\right)\end{array}\right)$$

$$= \frac{3^{\frac{-j-2}{2}}}{\sqrt{2}\,\Gamma(m-\alpha)}\left(\begin{array}{c}\left(\sqrt{3}-1\right)\left(\int_0^{\varepsilon_1} \frac{u^m(z)}{(\varepsilon_1 - z)^{\alpha-m+1}} dz - \int_0^{\varepsilon_1} \frac{u^m(z)}{(\varepsilon_3 - z)^{\alpha-m+1}} dz\right) \\ -\left(\sqrt{3}-1\right)\left(\int_{\varepsilon_1}^{\varepsilon_3} \frac{u^m(z)}{(\varepsilon_3 - z)^{\alpha-m+1}} dz\right) - 2\int_{\varepsilon_2}^{0} \frac{u^m(z)}{(\varepsilon_2 - z)^{\alpha-m+1}} dz\end{array}\right) \tag{55}$$

Taking modulus on both side of Equation 55 and appling the properties of modulus, we get Equation 56, 57, 58, 59, 60, 61 and 62

$$a_i| = \left| \frac{3^{\frac{-j-2}{2}}}{\sqrt{2}\,\Gamma(m-\alpha)} \begin{pmatrix} (\sqrt{3}-1)\left(\int_0^{\varepsilon_1} \frac{u^m(z)}{(\varepsilon_1 - z)^{\alpha-m+1}} dz - \int_0^{\varepsilon_1} \frac{u^m(z)}{(\varepsilon_3 - z)^{\alpha-m+1}} dz\right) \\ -(\sqrt{3}-1)\left(\int_{\varepsilon_1}^{\varepsilon_3} \frac{u^m(z)}{(\varepsilon_3 - z)^{\alpha-m+1}} dz\right) - 2\int_{\varepsilon_2}^{0} \frac{u^m(z)}{(\varepsilon_2 - z)^{\alpha-m+1}} dz \end{pmatrix} \right| \tag{56}$$

$$a_i| \leq \frac{3^{\frac{-j-2}{2}}}{\sqrt{2}\,\Gamma(m-\alpha)} \begin{bmatrix} (\sqrt{3}-1)\left|\int_0^{\varepsilon_1} \frac{u^m(z)}{(\varepsilon_1 - z)^{\alpha-m+1}} dz - \int_0^{\varepsilon_1} \frac{u^m(z)}{(\varepsilon_3 - z)^{\alpha-m+1}} dz\right| \\ +(\sqrt{3}-1)\left|\int_{\varepsilon_1}^{\varepsilon_3} \frac{u^m(z)}{(\varepsilon_3 - z)^{\alpha-m+1}} dz\right| + 2\left|\int_{\varepsilon_2}^{0} \frac{u^m(z)}{(\varepsilon_2 - z)^{\alpha-m+1}} dz\right| \end{bmatrix} \tag{57}$$

$$a_i| \leq \frac{3^{\frac{-j-2}{2}}}{\sqrt{2}\,\Gamma(m-\alpha)} \begin{bmatrix} (\sqrt{3}-1)\int_0^{\varepsilon_1} |u^m(z)|\left[\frac{1}{(\varepsilon_1 - z)^{\alpha-m+1}} - \frac{1}{(\varepsilon_3 - z)^{\alpha-m+1}}\right] dz \\ +(\sqrt{3}-1)\int_{\varepsilon_1}^{\varepsilon_3} |u^m(z)| \frac{1}{(\varepsilon_3 - z)^{\alpha-m+1}} dz + 2\int_{\varepsilon_2}^{0} |u^m(z)| \frac{1}{(\varepsilon_2 - z)^{\alpha-m+1}} dz \end{bmatrix} \tag{58}$$

$$|a_i| \leq \frac{3^{\frac{-j-2}{2}} M}{\sqrt{2}\,\Gamma(m-\alpha)} \begin{bmatrix} (\sqrt{3}-1)\int_0^{\varepsilon_1} \left[\frac{1}{(\varepsilon_1 - z)^{\alpha-m+1}} - \frac{1}{(\varepsilon_3 - z)^{\alpha-m+1}}\right] dz \\ +(\sqrt{3}-1)\int_{\varepsilon_1}^{\varepsilon_3} \frac{1}{(\varepsilon_3 - z)^{\alpha-m+1}} dz + 2\int_{\varepsilon_2}^{0} \frac{1}{(\varepsilon_2 - z)^{\alpha-m+1}} dz \end{bmatrix} \tag{59}$$

$$|a_i| \leq \frac{3^{\frac{-j-2}{2}} M}{\sqrt{2}\,\Gamma(m-\alpha)} \left[\frac{(\sqrt{3}-1)}{(m-\alpha)} \begin{bmatrix} (\varepsilon_3 - \varepsilon_1)^{m-\alpha} - {\varepsilon_3}^{m-\alpha} \\ +{\varepsilon_1}^{m-\alpha} + (\varepsilon_3 - \varepsilon_1)^{m-\alpha} \end{bmatrix} - 2{\varepsilon_2}^{m-\alpha}\right] \tag{60}$$

$m - \alpha > 0, \varepsilon_1 < \varepsilon_3 \Rightarrow {\varepsilon_1}^{m-\alpha} < {\varepsilon_3}^{m-\alpha} \Rightarrow {\varepsilon_1}^{m-\alpha} - {\varepsilon_3}^{m-\alpha} < 0\,, \varepsilon_2 > 0 \Rightarrow -2{\varepsilon_2}^{m-\alpha} < 0$

$\Rightarrow {\varepsilon_1}^{m-\alpha} - {\varepsilon_3}^{m-\alpha} - 2{\varepsilon_2}^{m-\alpha} < 0$

$$|a_i| \leq \frac{3^{\frac{-j-2}{2}} M}{\sqrt{2}\,\Gamma(m-\alpha)} \left[\frac{(\sqrt{3}-1)}{(m-\alpha)} [2(\varepsilon_3 - \varepsilon_1)^{m-\alpha}]\right] < \frac{4.3^{\frac{-j-2}{2}} M}{\sqrt{2}\,\Gamma(m-\alpha+1)}$$

$$= \frac{2\sqrt{2}\,3^{\frac{-j-2}{2}} M}{\Gamma(m-\alpha+1)} \times \frac{1}{3^{j(m-\alpha)}} \tag{61}$$

$$|a_i| \leq \frac{2\sqrt{2}\,M}{3\Gamma(m-\alpha+1)} \times \frac{1}{3^{j\left(m-\alpha+\frac{1}{2}\right)}} \tag{62}$$

Theorem 1: - If $u(x,t)$ represent the exact solution and $u_{3m}(x,t)$ represents the Scale 3 Haar wavelet-based approximated solution, then for a fixed value of $t = t_l$

$$\left\|E_j\right\| = \|u(x,t) - u_{3m}(x,t)\| \leq \frac{4\sqrt{2M}\;K\,|\Delta t|}{\Gamma(m-\alpha+1)}\left(\frac{3^{-j(m-\alpha+\frac{1}{2})}}{1-3^{-\left(m-\alpha-\frac{1}{2}\right)}}\right)$$

Proof. At j^{th} level of resolution, error estimation for the solution is given by

$$\left\|E_j\right\| = \|u(x,t) - u_{3m}(x,t)\| = \left|\Delta t * \sum_{i=3m+1}^{\infty} a_i (q_{i,2}(x) - x\,q_{i,2}(1))\right|$$

$$\left\|E_j\right\|^2 = |\Delta t|^2 * \left|\sum_{i=3m+1}^{\infty} a_i (q_{i,2}(x) - x\,q_{i,2}(1))\right|^2 =$$
$$\left|\int_{-\infty}^{\infty} \langle \sum_{i=3m+1}^{\infty} a_i (q_{i,2}(x) - x\,q_{i,2}(1)) \cdot \sum_{k=3m+1}^{\infty} a_k (q_{k,2}(x) - x\,q_{k,2}(1)) \rangle\right|$$

$$\leq |\Delta t|^2 * \left|\sum_{i=3m+1}^{\infty}\sum_{k=3m+1}^{\infty} \int_0^1 a_i a_k \left(q_{i,2}(x) - xq_{i,2}(1)\right)\left(q_{k,2}(x) - xq_{k,2}(1)\right) dx\right|$$

$$\leq |\Delta t|^2 * \left|a_i a_k\, M_{i,k}\right|$$

Where $M_{i,k} = \underset{i,k}{\text{Sup}} \int_0^1 \left(q_{i,2}(x) - xq_{i,2}(1)\right)\left(q_{k,2}(x) - xq_{k,2}(1)\right) dx$

$$\left\|E_j\right\|^2 \leq |\Delta t|^2 * \sum_{i=3m+1}^{\infty} \left| a_i (a_{3m} M_{i,3m} + a_{3m+1} M_{i,3m+1} + a_{3m+2} M_{i,3m+2} + a_{3m+3,} M_{i,3m+3} + \cdots) \right|$$

$$\leq |\Delta t|^2 * \sum_{i=3m+1}^{\infty} \left| a_i M_i (a_{3m} + a_{3m+1} + a_{3m+2} + a_{3m+3,} + \cdots)\right|$$

Where $M_i = \underset{i,k}{\text{Sup}}\, M_{i,k}$

Using Lemma 1 in the equation we get

$$\left\|E_j\right\|^2 \leq \frac{4\sqrt{2}K}{\Gamma(m-\alpha+1)} \frac{|\Delta t|^2 3^{-j(m-\alpha+\frac{1}{2})}}{1-3^{-\left(m-\alpha-\frac{1}{2}\right)}} \sum_{i=3m+1}^{\infty} |a_i M_i|$$

Take $M = \underset{i}{\text{Sup}}\, M_i$

$$\left\|E_j\right\|^2 \leq \cdot \frac{4\sqrt{2}\,K|\Delta t|^2}{\Gamma(m-\alpha+1)} \frac{M 3^{-j(m-\alpha+\frac{1}{2})}}{1-3^{-\left(m-\alpha-\frac{1}{2}\right)}} \sum_{i=3m+1}^{\infty} |a_i| = \frac{4\sqrt{2}\,K|\Delta t|^2}{\Gamma(m-\alpha+1)} \frac{M 3^{-j(m-\alpha+\frac{1}{2})}}{1-3^{-\left(m-\alpha-\frac{1}{2}\right)}} * \frac{4\sqrt{2}\,K}{\Gamma(m-\alpha+1)} \frac{3^{-j(m-\alpha+\frac{1}{2})}}{1-3^{-\left(m-\alpha-\frac{1}{2}\right)}}$$

$$\left\|E_j\right\| = \frac{4\sqrt{2M}\ K\ |\Delta t|}{\Gamma(m-\alpha+1)}\left(\frac{3^{-j\left(m-\alpha+\frac{1}{2}\right)}}{1-3^{-\left(m-\alpha-\frac{1}{2}\right)}}\right) \tag{63}$$

It is clear from the Equation 63 that error bound is inversely proportional to the level of resolution which means that with the increase in the level of resolution, error bound decreases i.e. $j \to \infty \Rightarrow \left\|E_j\right\| \longrightarrow 0$. This proves the convergence of solution u (x, t). In a similar way, the convergence of $v(x,t)$ solution can be proved. It ensures the stability of the solutions.

RESULTS AND DISCUSSIONS FROM NUMERICAL EXPERIMENT

To describe the appropriateness of the present scheme for fractional coupled Burgers' equation, solutions of two problems obtained by the present scheme had been analyzed and absolute errors were calculated to check the efficiency of the present scheme with the help of following formulas

Absolute error = $|u_{exact}(t_l) - u_{num}(t_l)|$

where t_i represents the collocation points of the domain.

Numerical Experiment No. 1: - Consider the following space-time fractional coupled Burgers' Equation 64

$$\begin{cases} \dfrac{\partial^\alpha u}{\partial t^\alpha} = \dfrac{\partial^2 u}{\partial x^2} + 2\,u\dfrac{\partial^\beta u}{\partial x^\beta} - \dfrac{\partial(uv)}{\partial x} \quad , \quad x \in [0\,,1] \quad , t \in [0,T] \\ \dfrac{\partial^\gamma v}{\partial t^\gamma} = \dfrac{\partial^2 v}{\partial x^2} + 2\,v\dfrac{\partial^\delta v}{\partial x^\delta} - \dfrac{\partial(uv)}{\partial x} \quad , \quad x \in [0\,,1] \quad , t \in [0,T] \end{cases} \tag{64}$$

Subjected to the boundary conditions given in Equation 65

$$u(0,t) = 0, u(1,t) = e^{-t}\sin 1\ \ ,\ v(0,t) = 0, v(1,t) = e^{-t}\sin 1\ \ \forall\ \ t \in [0,T] \tag{65}$$

and with the initial condition given in Equation 66

$$u(x,0) = \sin x \quad , \quad v(x,0) = \sin x \qquad \forall\ \ x \in [0\,,1] \tag{66}$$

The exact solution of the Equation 64 subjected to the conditions given in Equation 65 and 66 for $\alpha = \beta = \gamma = \delta = 1$ is

$$u(x,t) = e^{-t}\sin x \quad , \qquad v(x,t) = e^{-t}\sin x$$

The numerical solution obtained by applying the given methodology for Equation 64 subjected to the conditions given in Equation 65 and 66 is

$$u(x_l,t_{r+1}) = (t_{r+1} - t_r)\sum_{i=1}^{3m} a_i(q_{i,2}(x_l) - x_l q_{i,2}(1)) + \big(u(x_l,t_r) - f_1(t_r)\big)$$
$$+x_l\big(f_2(t_{r+1}) - f_1(t_{r+1})\big) - x_l\big(f_2(t_r) - f_1(t_r)\big) + f_1(t_{r+1})$$

$$v(x_l,t_{r+1}) = (t_{r+1} - t_r)\sum_{i=1}^{3m} b_i(q_{i,2}(x_l) - x_l q_{i,2}(1)) + \big(v(x_l,t_r) - \varphi_1(t_r)\big)$$
$$+x_l\big(\varphi_2(t_{r+1}) - \varphi_1(t_{r+1})\big) - x_l\big(\varphi_2(t_r) - \varphi_1(t_r)\big) + \varphi_1(t_{r+1})$$

at the various times by using successive iteration for $r = 0,1,2,3,\ldots$. The process of finding the solution in the discrete form starts by taking $r = 0, t_0 = 0$ and $f_1(t_r) = 0, f_2(t_r) = e^{-t_r}\sin 1$, $\varphi_1(t_r) = 0, \varphi_2(t_{r+1}) = e^{-t_r}\sin 1$ for $r = 0, t_0 = 0$ and rest all the values will be obtained using the iterative process.

Results obtained for example 1 are also reported by the way of figures and tables. It can be seen from Figure 1 and Figure 2 that the solution obtained by the proposed method for the case (when $\alpha = \beta = \gamma = \delta = 1$) is in good agreement with the analytical solution available in the literature. Table 1 and Figure 3 show the absolute errors in the results obtained at the different collocation points for the case $\alpha = \beta = \gamma = \delta = 1$ and it is of order 10^{-5} which assures the efficiency and reliability of the proposed method. In Table 2, results obtained by the present method are compared with another method (Ray, 2013) available in the literature and it is found that the present method outperforms over another method available in the literature. Table 3 explains the absolute error in the solution for different values of Δt which illustrate the direct dependence of absolute error on meshsize for time variable. For better visibility contour plots and 2D-solution plots are also given in Figure 4 and Figure 5. Most important fact has been explained by the Figure 6 and Figure 7 that when we shift from one classical order derivative (integer-order 0) to another classical order derivative (integer-order 1) in the coupled Burgers' equation the behavior of the solution does not remain the same, in fact many variations have been observed in the solution space with the variation in the order of time derivative or space derivative which gives the better insight of microscopic behavior of poly-dispersive sedimentation phenomena of two different types of particle concentration in the fluid.

Table 1

Absolute error in numerical results u(x,t) at collocation points for integer order $\alpha = \beta = \gamma = \delta = 1$ with $\eta = \xi = -2$, $\mu = \lambda = 1$ and $\Delta t = 0.1$

Time (t) \ x	**0.0556**	**0.1667**	**0.2778**	**0.3889**	**0.5**	**0.6111**	**0.7222**	**0.8333**	**0.9444**
0.1	2.30×10^{-5}	5.82×10^{-5}	9.26×10^{-5}	1.24×10^{-4}	1.52×10^{-4}	1.76×10^{-4}	1.97×10^{-4}	2.15×10^{-4}	2.30×10^{-4}
0.2	6.66×10^{-5}	1.69×10^{-4}	2.68×10^{-4}	3.59×10^{-4}	4.39×10^{-4}	5.09×10^{-4}	5.70×10^{-4}	6.22×10^{-4}	6.67×10^{-4}
0.3	1.04×10^{-4}	2.62×10^{-4}	4.16×10^{-4}	5.56×10^{-4}	6.80×10^{-4}	7.88×10^{-4}	8.82×10^{-4}	9.63×10^{-4}	1.03×10^{-3}
0.4	1.30×10^{-4}	3.27×10^{-4}	5.19×10^{-4}	6.93×10^{-4}	8.47×10^{-4}	9.82×10^{-4}	1.10×10^{-3}	1.20×10^{-3}	1.29×10^{-3}
0.5	1.42×10^{-4}	3.57×10^{-4}	5.64×10^{-4}	7.53×10^{-4}	9.20×10^{-4}	1.07×10^{-3}	1.19×10^{-3}	1.30×10^{-3}	1.39×10^{-3}
0.6	1.38×10^{-4}	3.44×10^{-4}	5.44×10^{-4}	7.25×10^{-4}	8.85×10^{-4}	1.03×10^{-3}	1.15×10^{-3}	1.25×10^{-3}	1.34×10^{-3}
0.7	1.17×10^{-4}	2.89×10^{-4}	4.55×10^{-4}	6.06×10^{-4}	7.40×10^{-4}	8.57×10^{-4}	9.58×10^{-4}	1.04×10^{-3}	1.12×10^{-3}
0.8	7.87×10^{-5}	1.94×10^{-4}	3.05×10^{-4}	4.05×10^{-4}	4.94×10^{-4}	5.72×10^{-4}	6.39×10^{-4}	6.97×10^{-4}	7.46×10^{-4}
0.9	2.80×10^{-5}	6.86×10^{-5}	1.08×10^{-4}	1.43×10^{-4}	1.74×10^{-4}	2.02×10^{-4}	2.25×10^{-4}	2.46×10^{-4}	2.63×10^{-4}

Table 2

Comparision of Numerical results at Random collocation Points available in Literature for Experiment. No.1 at integer-order $\alpha = \beta = \gamma = \delta = 1$ with $\eta = \xi = -2$, $\mu = \lambda = 1$ and $\Delta t = 0.1$

Collocation Points (x,t)	Exact Solution $u(x,t) = v(x,t) = e^{-t}\sin x$	Numerical Solution $u(x,t)$	Numerical Solution $v(x,t)$	Scale 3 Haar wavelet method (Absolute Error)	Reduced differential Transform method (Absolute Error) (Ray, 2013)
(0.1,0.1)	0.090333	0.090329	0.090329	4.09×10^{-6}	1.62×10^{-5}
(0.2,0.2)	0.162657	0.162730	0.162730	7.38×10^{-5}	2.52×10^{-4}
(0.3,0.3)	0.218927	0.219199	0.219199	2.73×10^{-4}	1.24×10^{-3}
(0.4,0.4)	0.261035	0.261596	0.261596	5.61×10^{-4}	3.77×10^{-3}
(0.5,0.5)	0.290786	0.291659	0.291659	8.73×10^{-4}	8.86×10^{-3}
(0.6,0.6)	0.309882	0.311006	0.311006	1.12×10^{-3}	1.76×10^{-2}
(0.7,0.7)	0.319909	0.321135	0.321135	1.23×10^{-3}	3.11×10^{-2}
(0.8,0.8)	0.322329	0.323434	0.323434	1.11×10^{-3}	5.07×10^{-2}
(0.9,0.9)	0.318477	0.319182	0.319182	7.05×10^{-4}	7.71×10^{-2}

Table 3
Maximum absolute error in numerical results u(x,t) and v(x,t) at the integer order α= β= γ= δ =1 with η= ξ = -2, μ=λ=1 for different values of Δt

Δt	$\|\boldsymbol{E}(\boldsymbol{u})\|_\infty$	$\|\boldsymbol{E}(\boldsymbol{v})\|_\infty$
0.0100	1.22142096728672410^{-4}	1.22142096728672410^{-4}
0.0010	$2.218389533070741\times10^{-6}$	$2.218389533070741\times10^{-6}$
0.0001	2.41311621795858910^{-8}	2.41311621795858910^{-8}

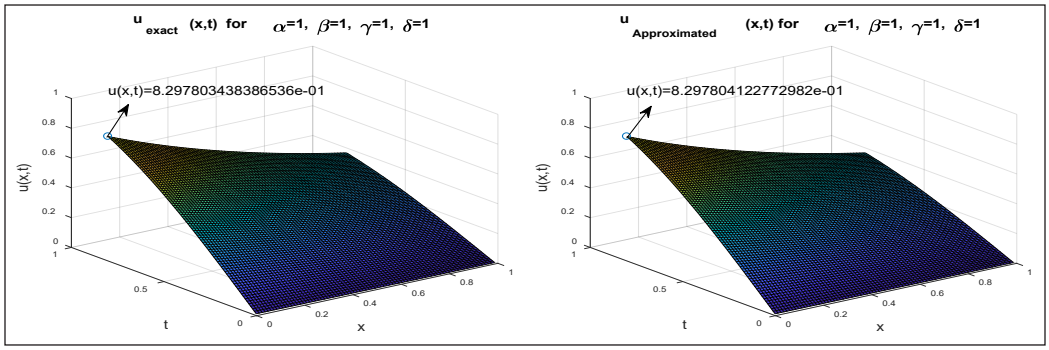

Figure 1. 3D Graphical representation of exact and approximated solution u(x,t) of Experiment No. 1 for integer order α= β= γ= δ =1 with η= ξ = -2, μ=λ=1 and Δt = 0.01

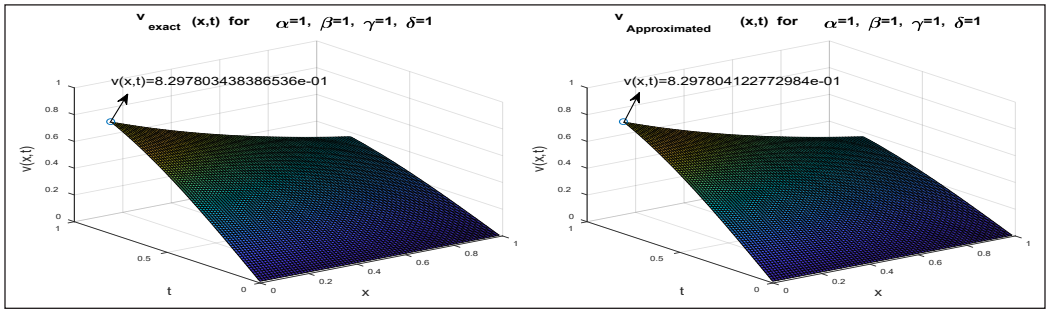

Figure 2. 3D Graphical representation of exact and approximated solution v(x,t) of Experiment No. 1 at integer order α= β= γ= δ =1 with η= ξ = -2, μ=λ=1 and Δt = 0.01

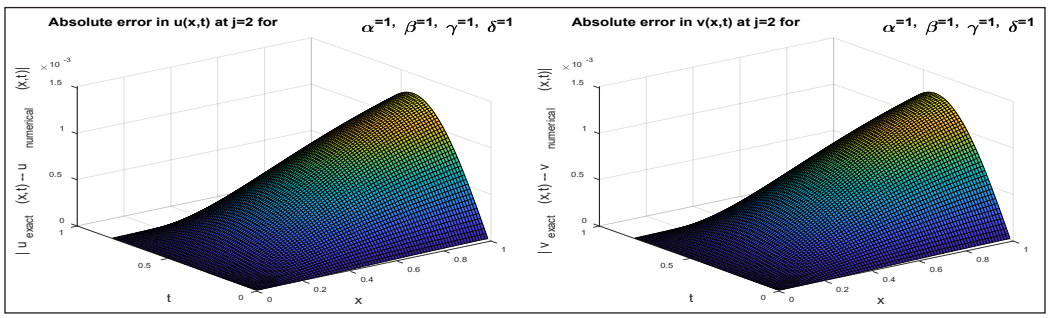

Figure 3. Surface plot of absolute error in the solutions u(x,t) and v(x,t) of Experiment No. 1 for j=3 at the integer order α= β= γ= δ =1 with η= ξ = -2, μ=λ=1 and Δt = 0.01

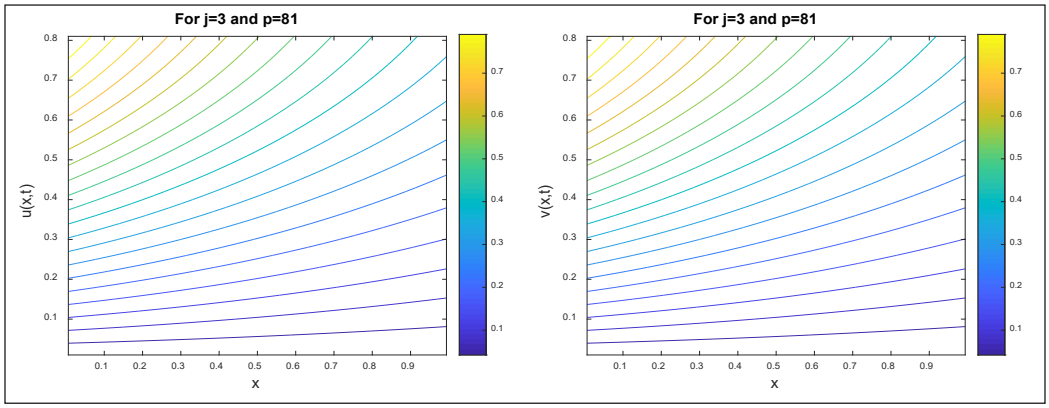

Figure 4. Contour representation of solutions u(x,t) and v(x,t) of Experiment No. 1 at the integer order α= β= γ= δ =1 with η= ξ = -2, μ=λ=1 and Δt = 0.01

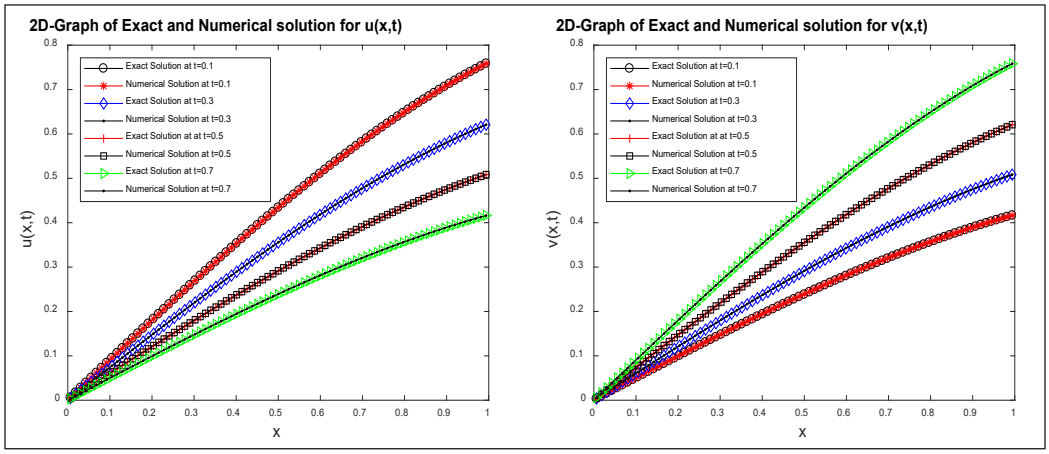

Figure 5. 2D-Graphical representation of exact and approximated solutions u(x,t) and v(x,t) of Experiment No. 2 for different values of t at the integer order α= β= γ= δ =1 with η= ξ = -2, μ=λ=1 and Δt = 0.01

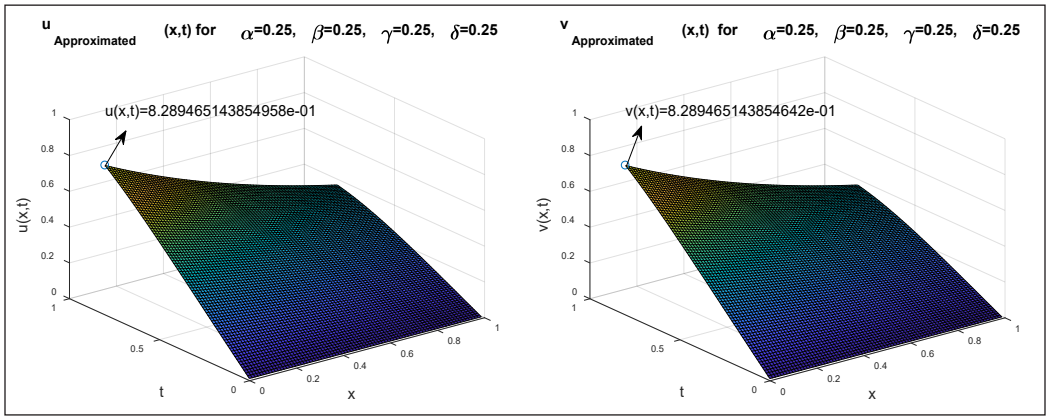

Figure 6. Approximate solution of Experiment No. 1 in 3D with different values of α, β ∈ (0,1] and fixed values of γ= δ =0.25 with η= ξ = -2, μ=λ=1 and Δt = 0.001

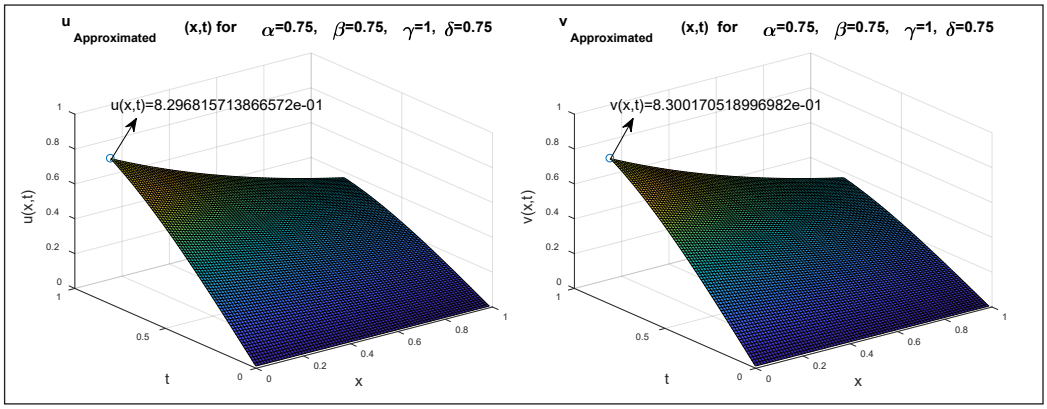

Figure 7. Approximate solution of Experiment No. 1 in 3D with different values of α, β, γ, δ ∈ (0,1] for which the solution behaves differently at η= ξ = -2, μ=λ=1 and Δt = 0.01.

Numerical Experiment No. 2: - Consider the following space-time fractional coupled Burgers' Equation 67

$$\begin{cases} \dfrac{\partial^{\alpha} u}{\partial t^{\alpha}} = \dfrac{\partial^2 u}{\partial x^2} + 2\,u\dfrac{\partial^{\beta} u}{\partial x^{\beta}} - \dfrac{\partial (uv)}{\partial x} \quad , \qquad x \in [0\,,1] \quad , t \in [0,T \\ \dfrac{\partial^{\gamma} v}{\partial t^{\gamma}} = \dfrac{\partial^2 v}{\partial x^2} + 2\,v\dfrac{\partial^{\delta} v}{\partial x^{\delta}} - \dfrac{\partial (uv)}{\partial x} \quad , \qquad x \in [0\,,1] \quad , t \in [0,T \end{cases} \tag{67}$$

Subjected to the boundary conditions given in Equation 68

$$u(0,t) = 0, u(1,t) = 0, v(0,t) = 0, v(1,t) = 0 \qquad \forall \quad t \in [0,T] \tag{68}$$

and with the initial condition given in Equation 69

$$u(x,0) = \sin(2\pi x - \pi) \quad , \qquad v(x,0) = \sin(2\pi x - \pi) \qquad \forall \quad \mathrm{x} \in [0\,,1] \tag{69}$$

Analytic solution of Equation 67 when $\alpha = \beta = \gamma = \delta = 1$ is given by Equation 70 as

$$u(x,t) = e^{-4\pi^2 t}\sin(2\pi x - \pi) \quad , \qquad v(x,t) = e^{-4\pi^2 t}\sin(2\pi x - \pi) \tag{70}$$

The numerical solution obtained by applying the given methodology is

$$u(x_l, t_{r+1}) = (t_{r+1} - t_r)\sum_{i=1}^{3m} a_i (q_{i,2}(x_l) - x_l\, q_{i,2}(1)) + \big(u(x_l, t_r) - f_1(t_r)\big) + x_l\big(f_2(t_{r+1}) - f_1(t_{r+1})\big) - x_l\big(f_2(t_r) - f_1(t_r)\big) + f_1(t_{r+1})$$

$$v(x_l,t_{r+1}) = (t_{r+1} - t_r)\sum_{i=1}^{3m} b_i(q_{i,2}(x_l) - x_l q_{i,2}(1)) + \big(v(x_l,t_r) - \varphi_1(t_r)\big)$$
$$+x_l\big(\varphi_2(t_{r+1}) - \varphi_1(t_{r+1})\big) - x_l\big(\varphi_2(t_r) - \varphi_1(t_r)\big) + \varphi_1(t_{r+1})$$

at various times by using successive iteration for $r = 0,1,2,3,\ldots$ where $f_1(t_r) = 0, f_2(t_r) = 0, \varphi_1(t_r) = 0, \varphi_2(t_r) = 0$ for $r = 0, t_0 = 0$ and rest all the values will be obtained using the iterative process.

Table 4 explains the absolute errors in the results obtained by the proposed method for example 2 by considering the domain $x \in [0,1]$ and $\Delta t = 0$ and it is of order 10^{-5} which assures the efficiency and reliability of the proposed method. It can be seen from Figure 8 to Figure 14 that the solution obtained by the proposed method for the case (when$\alpha = \beta = \gamma = \delta = 1$ is in good agreement with the analytical solution available in

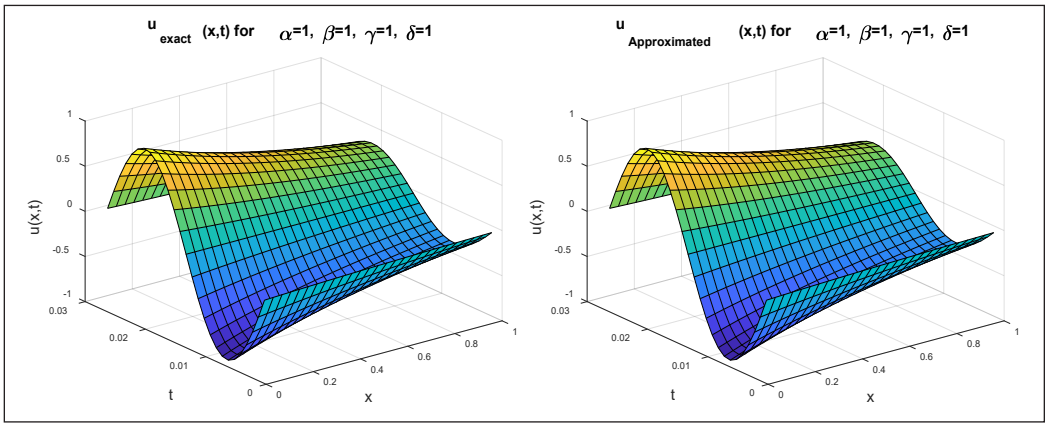

Figure 8. 3D Graphical representation of exact and approximated solution u(x,t) of Experiment No. 2 at integer order α= β= γ= δ =1 with η= ξ = -2, μ=λ=1 and Δt = 0.001

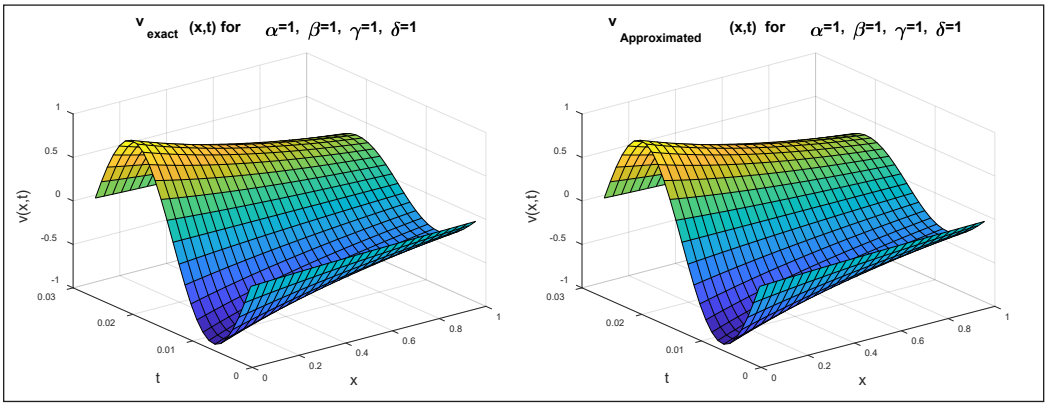

Figure 9. 3D Graphical representation of exact and approximated solution v(x,t) of Experiment No. 2 at integer order α= β= γ= δ =1 with η= ξ = -2, μ=λ=1 and Δt = 0.001

Table 4
Absolute error in numerical results u(x,t) at random collocation points for integer order α= β= γ= δ =1 with η= ξ = -2, μ=λ=1

t \ x	0.05556	0.16667	0.27778	0.38889	0.50000	0.61111	0.72222	0.83333	0.94444
0.1	6.67×10^{-5}	4.35×10^{-5}	3.22×10^{-5}	$2.62\times\times10^{-5}$	2.25×10^{-5}	1.99×10^{-5}	1.81×10^{-5}	1.67×10^{-5}	1.56×10^{-5}
0.2	1.69×10^{-4}	1.10×10^{-4}	8.17×10^{-5}	6.64×10^{-5}	5.69×10^{-5}	5.05×10^{-5}	4.58×10^{-5}	4.23×10^{-5}	3.95×10^{-5}
0.3	1.92×10^{-4}	1.25×10^{-4}	9.29×10^{-5}	7.55×10^{-5}	6.47×10^{-5}	5.74×10^{-5}	5.21×10^{-5}	4.81×10^{-5}	4.49×10^{-5}
0.4	1.25×10^{-4}	8.18×10^{-5}	6.06×10^{-5}	4.93×10^{-5}	4.22×10^{-5}	3.75×10^{-5}	3.40×10^{-5}	3.14×10^{-5}	2.93×10^{-5}
0.5	2.89×10^{-19}	6.44×10^{-19}	1.05×10^{-18}	1.04×10^{-18}	9.44×10^{-19}	9.33×10^{-19}	1.52×10^{-18}	1.11×10^{-19}	9.49×10^{-19}
0.6	1.25×10^{-4}	8.18×10^{-5}	6.06×10^{-5}	4.93×10^{-5}	4.22×10^{-5}	3.75×10^{-5}	3.40×10^{-5}	3.14×10^{-5}	2.93×10^{-5}
0.7	1.92×10^{-4}	1.25×10^{-4}	9.29×10^{-5}	7.55×10^{-5}	6.47×10^{-5}	5.74×10^{-5}	5.21×10^{-5}	4.81×10^{-5}	4.49×10^{-5}
0.8	1.69×10^{-4}	1.10×10^{-4}	8.17×10^{-5}	6.64×10^{-5}	5.69×10^{-5}	5.05×10^{-5}	4.58×10^{-5}	4.23×10^{-5}	3.95×10^{-5}
0.9	6.67×10^{-5}	4.35×10^{-5}	3.22×10^{-5}	2.62×10^{-5}	2.25×10^{-5}	1.99×10^{-5}	1.81×10^{-5}	1.67×10^{-5}	1.56×10^{-5}

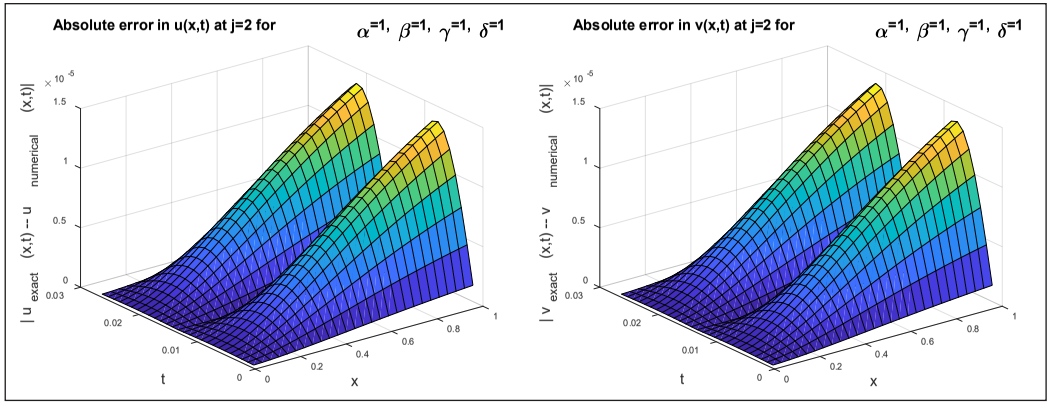

Figure 10. Surface plot of absolute error in the solutions u(x,t) and v(x,t) of Experiment No. 2 for j=2 at the integer order α= β= γ= δ =1 with η= ξ = -2, μ=λ=1 and Δt = 0.001

the literature. Table 5 explains the absolute error in the solution for different values of Δt which illustrate the direct dependence of absolute error on meshsize for time variable. It can also be observed from the Figure 13 and Figure 14 that whenever we are changing the values of γ and δ by fixing the values of α, β, we are getting the change in the solution

Table 5
Maximum absolute error in numerical results u(x,t) and v(x,t) at the integer order α= β= γ= δ =1 with η= ξ = -2, μ=λ=1 for different values of Δt

Δt	$\|\boldsymbol{E}(\boldsymbol{u})\|_\infty$	$\|\boldsymbol{E}(\boldsymbol{v})\|_\infty$
0.0100	$2.09861158048527\times10^{-4}$	$2.098611580485271\times10^{-4}$
0.0010	$3.764653977598853\times10^{-6}$	$3.764653977598853\times10^{-6}$
0.0001	$6.090606685656975\times10^{-8}$	$6.090606685656975\times10^{-8}$

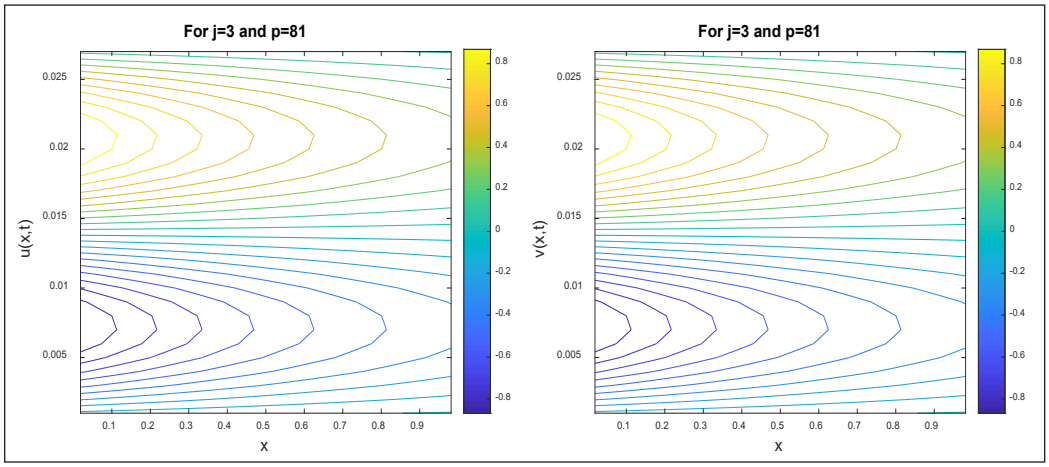

Figure 11. Contour representation of solutions u(x,t) and v(x,t) of Experiment No. 2 at the integer order α= β= γ= δ =1 with η= ξ = -2, μ=λ=1 and Δt = 0.001

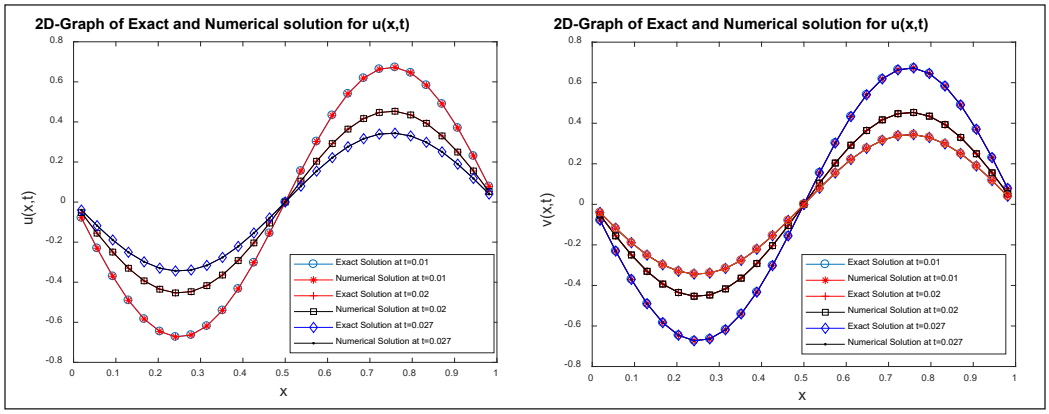

Figure 12. 2D-Graphical representation of exact and approximated solutions u(x,t) and v(x,t) of Experiment No. 2 for different values of t at the integer order α= β= γ= δ =1 with η= ξ = -2, μ=λ=1 and Δt = 0.001

space of $v(x,t)$ and there is no change in the solution space of $u(x,t)$ and *vice versa*. It is because of the reason that α, β are orders of the time and space fractional derivatives of $u(x,t)$ respectively and that γ, δ are orders of the time and space fractional derivatives of $u(x,t)$ respectively which explains the importance of fractional models in explaining the microscopic behavior of the phenomenon .

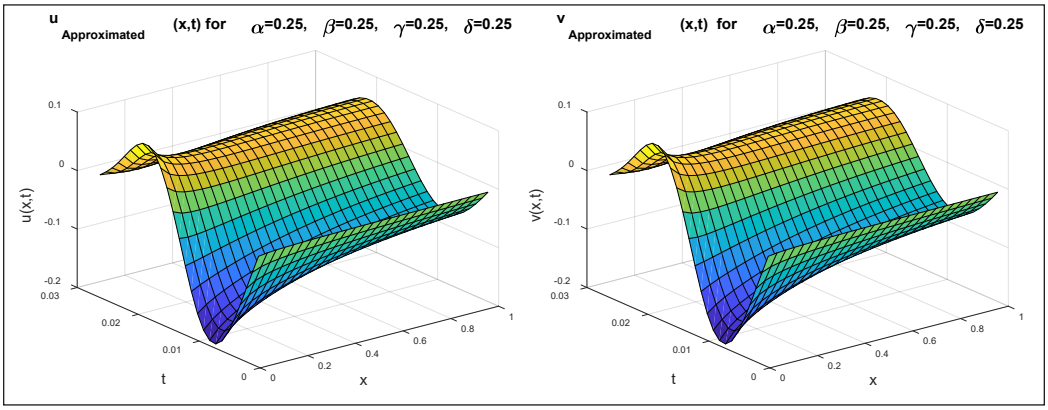

Figure 13. Approximate solution of Experiment No. 2 in 3D with different values of γ, δ ∈ (0,1] and fixed values of α=β= 0.25 with η= ξ = -2, μ=λ=1 and Δt = 0.001

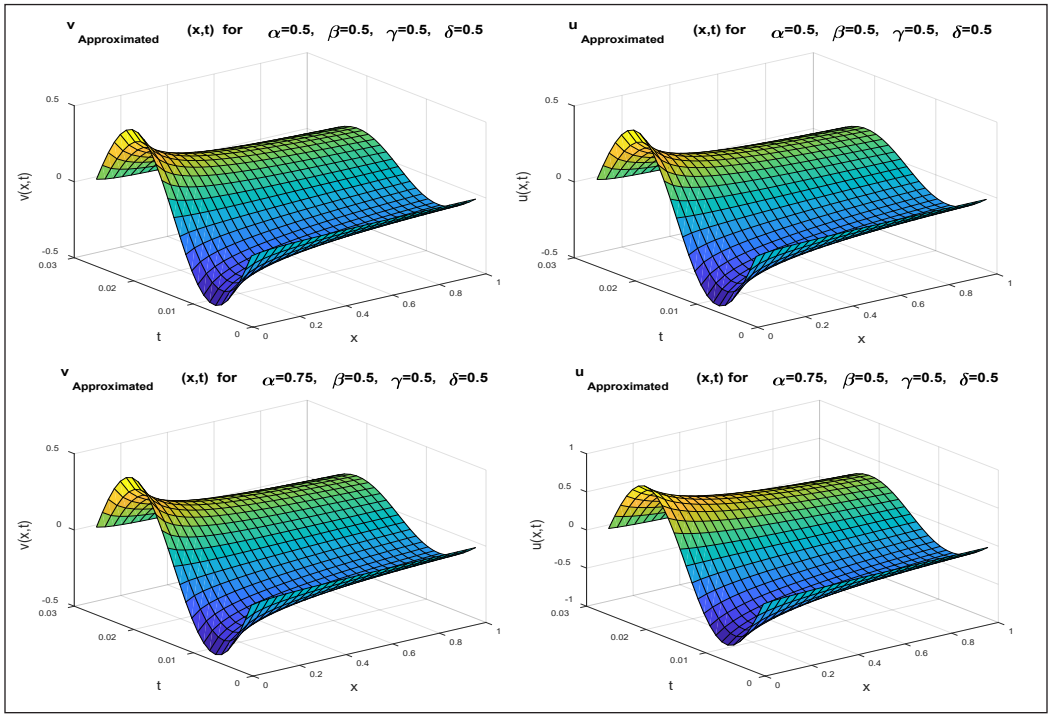

Figure 14. Approximate solution of Experiment No. 2 in 3D with different values of α, β ∈ (0,1] and fixed values of γ= δ =0.5 with η= ξ = -2, μ=λ=1 and Δt = 0.001

CONCLUSION

We have developed a scale 3 Haar wavelet-based collocation scheme to find the solution of nonlinear coupled fractional differential equations. Two examples of space-time fractional coupled Burgers' equation with different boundary and initial constraints were considered to prove the reliability and efficiency of the proposed numerical scheme. It had been observed in with the help of MATLAB stimulation and computations that solution was behaving differentially as we varied the order of fractional derivatives in space-time fractional coupled Burgers' equation and giving the accuracy of order 10^{-5} at integer-order derivative (i.e. at $\alpha = \beta = \gamma = \delta = 1$) for j=2 which demonstrated the performance of the scheme.The proposed method was compared with another method available in the literature and it was found that the proposed method was working better than the other method. Looking at the performance of the method for the given set of numerical experiments, the proposed method can be extended to explain the behavior of the different phenomenon by solving the system of fractional differential equations governing those phenomena. The proposed method provides an insight into the microscopic behavior of phenomena under study. The given method is also fully supportive and compatible with the ordinary, partial, fractional differential equations and integral equations.

ACKNWOLEDGEMENT

We thank the anonymous reviewers and editors for their useful suggestion to develop this manuscript.

REFERENCES

Abuasad, S., Moaddy, K., & Hashim, I. (2019). Analytical treatment of two-dimensional fractional Helmholtz equations. *Journal of King Saud University-Science, 31*(4), 659-666.

Atangana, A. (2016). On the new fractional derivative and application to nonlinear Fisher ' s reaction – diffusion equation. *Applied Mathematics and Computation*, *273*, 948-956.

Baleanu, D., Inc, M., Yusuf, A., & Aliyu, A. I. (2018). Lie symmetry analysis, exact solutions and conservation laws for the time fractional Caudrey–Dodd–Gibbon–Sawada–Kotera equation. *Communications in Nonlinear Science and Numerical Simulation*, *59*, 222-234.

Bezerra, F. D. M., Carvalho, A. N., Dlotko, T., & Nascimento, M. J. D. (2018). Fractional Schrödinger equation; solvability and connection with classical Schrödinger equation. *Journal of Mathematical Analysis and Applications*, *457*(1), 336-360.

Chen, Y., & An, H. L. (2008). Numerical solutions of coupled Burgers equations with time- and space-fractional derivatives. *Applied Mathematics and Computation*, *200*(2008), 87-95.

Chui, C. K., & Lian, J. A. (1995). Construction of compactly supported symmetric and antisymmetric orthonormal wavelets with scale 3. *Applied and Computational Harmonic Analysis*, *2*(1), 21-51.

Das, S. (2011). *Functional fractional calculus*. Heidelberg, Germany: Springer-Verlag.

Duan, J. S., Lu, L., Chen, L., & An, Y. L. (2017). Fractional model and solution for the Black-Scholes equation. *Mathematical Methods in the Applied Sciences*, *41*(2), 697-704.

Esipov, S. E. (1995). Coupled Burgers equations: A model of polydispersive sedimentation. *Physical Review E*, *52*(4), 3711-3718.

Heydari, M. H., Hooshmandasl, M. R., Ghaini, F. M., & Fereidouni, F. (2013). Two-dimensional Legendre wavelets for solving fractional Poisson equation with Dirichlet boundary conditions. *Engineering Analysis with Boundary Elements*, *37*(11), 1331-1338.

Hosseini, K., Mayeli, P., & Ansari, R. (2018). Bright and singular soliton solutions of the conformable time-fractional Klein–Gordon equations with different nonlinearities. *Waves in Random and Complex Media*, *28*(3), 426-434.

Inc, M. (2008). The approximate and exact solutions of the space- and time-fractional Burgers equations with initial conditions by variational iteration method. *Journal of Mathematical Analysis and Applications*, *345*(1), 476-484.

Inc, M., Yusuf, A., Aliyu, A. I., & Baleanu, D. (2018). Time-fractional Cahn–Allen and time-fractional Klein–Gordon equations: Lie symmetry analysis, explicit solutions and convergence analysis. *Physica A: Statistical Mechanics and Its Applications*, *493*, 94-106.

Karayer, H., Demirhan, D., & Buyukkilic, F. (2018). Solutions of local fractional sine-Gordon equations. *Waves in Random and Complex Media*, *5030*, 1-9.

Khan, N. A., Ara, A., & Mahmood, A. (2012). Numerical solutions of time-fractional Burgers equations: A comparison between generalized differential transformation technique and homotopy perturbation method. *International Journal of Numerical Methods for Heat and Fluid Flow*, *22*(2), 175-193.

Kumar, D., Singh, J., & Baleanu, D. (2018). A new numerical algorithm for fractional Fitzhugh–Nagumo equation arising in transmission of nerve impulses. *Nonlinear Dynamics*, *91*(1), 307-317.

Liu, J., & Hou, G. (2011). Numerical solutions of the space- and time-fractional coupled Burgers equations by generalized differential transform method. *Applied Mathematics and Computation*, *217*(16), 7001-7008.

Lopes, A. M., Machado, J. T., Pinto, C. M., & Galhano, A. M. (2013). Fractional dynamics and MDS visualization of earthquake phenomena. *Computers and Mathematics with Applications*, *66*(5), 647-658.

Lu, C., Fu, C., & Yang, H. (2018). Time-fractional generalized Boussinesq equation for Rossby solitary waves with dissipation effect in stratified fluid and conservation laws as well as exact solutions R. *Applied Mathematics and Computation*, *327*, 104-116.

Mahdy, A. M. S., & Marai, G. M. A. (2018). Numerical solution for the time-fractional Fokker-Planck equation using fractional power series method and the shifted Chebyshev polynomials of the third kind. *International Journal of Applied Engineering Research*, *13*(1), 366-374.

Mittal, R. C., & Pandit, S. (2018a). Sensitivity analysis of shock wave Burgers' equation via a novel algorithm based on scale-3 Haar wavelets. *International Journal of Computer Mathematics, 95*(3), 601-625.

Mittal, R. C., & Pandit, S. (2018b). Quasilinearized scale-3 Haar wavelets-based algorithm for numerical simulation of fractional dynamical systems. *Engineering Computations*, *35*(5), 1907-1931.

Mittal, R. C., & Pandit, S. (2019). New Scale-3 Haar Wavelets Algorithm for Numerical Simulation of Second Order Ordinary Differential Equations. *Proceedings of the National Academy of Sciences, India Section A: Physical Sciences, 89*(4), 799-808.

Mohebbi, A. (2018). Fast and high-order numerical algorithms for the solution of multidimensional nonlinear fractional Ginzburg-Landau equation. *European Physical Journal Plus*, *133*(2), 67-79.

Momani, S. (2005). Analytic and approximate solutions of the space- and time-fractional telegraph equations. *Applied Mathematics and Computation*, *170*(2005), 1126-1134.

Momani, S., & Odibat, Z. (2006a). Analytical approach to linear fractional partial differential equations arising in fluid mechanics. *Physics Letters, Section A: General, Atomic and Solid State Physics*, *355*(4-5), 271-279.

Momani, S., & Odibat, Z. (2006b). Analytical solution of a time-fractional Navier-Stokes equation by Adomian decomposition method. *Applied Mathematics and Computation*, *177*(2), 488-494.

Momani, S., & Shawagfeh, N. (2006). Decomposition method for solving fractional Riccati differential equations. *Applied Mathematics and Computation*, *182*(2006), 1083-1092.

Odibat, Z. M., & Momani, S. (2006). Approximate solutions for boundary value problems of time-fractional wave equation. *Applied Mathematics and Computation, 181*(1), 767-774.

Odibat, Z., & Momani, S. (2009). The variational iteration method: An efficient scheme for handling fractional partial differential equations in fluid mechanics. *Computers and Mathematics with Applications*, *58*(11), 2199-2208.

Povstenko, Y. Z. (2009). Thermoelasticity that uses fractional heat conduction equation. *Journal of Mathematical Sciences*, *162*(2), 296-305.

Prakash, A., Kumar, M., & Sharma, K. K. (2015). Numerical method for solving fractional coupled Burgers equations. *Applied Mathematics and Computation*, *260*(2015), 314-320.

Ray, S. S. (2012). On Haar wavelet operational matrix of general order and its application for the numerical solution of fractional Bagley Torvik equation. *Applied Mathematics and Computation*, *218*, 5239-5248.

Ray, S. S. (2013). Numerical solutions of (1 + 1) dimensional time fractional coupled Burger equations using new coupled fractional reduced differential transform method. *International Journal of Computing Science and Mathematics*, *4*(1), 1-15.

Ray, S. S., & Patra, A. (2013). Haar wavelet operational methods for the numerical solutions of fractional order nonlinear oscillatory Van der Pol system. *Applied Mathematics and Computation*, *220*, 659-667.

Roy, R., Akbar, M. A., & Majid, A. (2018). Exact wave solutions for the nonlinear time fractional Sharma – Tasso – Olver equation and the fractional Klein – Gordon equation in mathematical physics. *Optical and Quantum Electronics, 50*(1), 1-19.

Sahoo, P. K., & Riedel, T. (1998). *Mean value theorems and functional equations*. Singapore: World Scientific Publishing Co. Pte. Ltd.

Shen, T., Xin, J., & Huang, J. (2018). Time-space fractional stochastic Ginzburg-Landau equation driven by Gaussian white noise. *Stochastic Analysis and Applications*, *36*(1), 103-113.

Singh, J., Gupta, P. K., & Rai, K. N. (2011). Solution of fractional bioheat equations by finite difference method and HPM. *Mathematical and Computer Modelling*, *54*(9-10), 2316-2325.

Tawfik, A. M., Fichtner, H., Schlickeiser, R., & Elhanbaly, A. (2018). Analytical solutions of the space–time fractional Telegraph and advection–diffusion equations. *Physica A: Statistical Mechanics and Its Applications*, *491*, 810-819.

Tripathi, D., Pandey, S. K., & Das, S. (2010). Peristaltic flow of viscoelastic fluid with fractional Maxwell model through a channel. *Applied Mathematics and Computation*, *215*(10), 3645-3654.

Wang, Q. (2006). Numerical solutions for fractional KdV – Burgers equation by Adomian decomposition method. *Applied Mathematics and Computation*, *182*(2006), 1048-1055.

Yildirim, A., & Kelleci, A. (2010). Homotopy perturbation method for numerical solutions of coupled Burgers equations with time-and space-fractional derivatives. *International Journal of Numerical Methods for Heat and Fluid Flow*, *20*(8), 897-909.

Zahle, M., & Ziezold, H. (1996). Fractional derivatives of Weierstrass-type functions. *Journal of Computational and Applied Mathematics*, *76*(1996), 265-275.

Zhang, H., Jiang, X., & Yang, X. (2018). A time-space spectral method for the time-space fractional Fokker–Planck equation and its inverse problem. *Applied Mathematics and Computation*, *320*, 302-318.

Zhang, X., He, Y., Wei, L., Tang, B., & Wang, S. (2014). A fully discrete local discontinuous Galerkin method for one-dimensional time-fractional Fisher ' s equation. *International Journal of Computer Mathematics*, *91*(9), 2021-2038.